Lacticaseibacillus rhamnosus P118 enhances host tolerance to *Salmonella* infection by promoting microbe-derived indole metabolites

Baikui Wang[1,#], Xianqi Peng[2,3,#], Xiao Zhou[6], Xiuyan Jin[3], Abubakar Siddique[3], Jiayun Yao[2], Haiqi Zhang[2], Weifen Li[5], Yan Li[3,4], Min Yue[1,3,4,*]

1 Key Laboratory of Systems Health Science of Zhejiang Province, School of Life Science, Hangzhou Institute for Advanced Study, University of Chinese Academy of Sciences, Hangzhou 310024, China

2 Zhejiang Institute of Freshwater Fisheries, Ministry of Agriculture and Rural Affairs Key Laboratory of Healthy Freshwater Aquaculture, Key Laboratory of Fish Health and Nutrition of Zhejiang Province, Key Laboratory of Fishery Environment and Aquatic Product Quality and Safety of Huzhou City, Huzhou 313001, China

3 Department of Veterinary Medicine, Zhejiang University College of Animal Sciences, Hangzhou 310058, China

4 Hainan Institute of Zhejiang University, Sanya 572025, China

5 Institute of Animal Nutrition and Feed Sciences, Zhejiang University College of Animal Sciences, Hangzhou 310058, China

6. Ningbo Academy of Agricultural Sciences, Ningbo 315040, China

ORCID: Min Yue, https://orcid.org/0000-0002-6787-0794; Baikui Wang, https://orcid.org/0000-0001-5283-7337; Xianqi Peng, https://orcid.org/0000-0001-7143-8307

*** Corresponding Author: Professor Min Yue** (myue@zju.edu.cn)

[#] Baikui Wang and Xianqi Peng contributed equally to this work.

Abstract

Salmonella is one of the most common foodborne pathogens, resulting in inflammatory gastroenteritis and frequently accompanied by dysbiosis. Gut commensals, such as *Lactobacillus* species, have been proven to exhibit broad anti-bacterial activities and protect hosts against pathogenic infections. Here, *Lacticaseibacillus rhamnosus* strain P118, screened from 290 isolates recovered from fermented yoghurts and healthy piglet intestines using traditional and *Caenorhabditis elegans*-infection screening strategies, exerts great probiotic properties. Notably, P118 and its supernatant exhibited great antibacterial activities and attenuated *C. elegans* susceptibility to *Salmonella* infection. We found that P118 protected mice against *Salmonella* lethal infections by enhancing colonization resistance, reducing pathogen invasion, alleviating intestinal pro-inflammatory response, and improving microbial dysbiosis and fecal metabolite changes. Microbiota and fecal metabolome analyses suggested P118 administration significantly decreased the relative abundances of potentially harmful microbes (e.g., *Salmonella*, *Anaeroplasma*, *Klebsiella*) and increased the fecal levels of tryptophan and its derivatives (indole, indole-3-acrylic acid, 5-hydroxytryptophan, 5-methoxyindoleacetate). Deterministic processes determined the gut microbial community assembly of P118-pretreated mice. Integrated omics further demonstrated that P118 probiotic activities in enhancing host tolerance to *Salmonella* infection were mediated by microbe-derived tryptophan/indole metabolites (e.g., indole-3-acrylic acid, indole, tryptophan, 5-methoxyindoleacetic acid, and 5-hydroxytryptophan). Collective results demonstrate that *L. rhamnosus* P118 could enhance host tolerance to *Salmonella*

infections via various pathways, including direct antibacterial actions, inhibiting *Salmonella* colonization and invasion, attenuating pro-inflammatory responses of intestinal macrophages, and modulating gut microbiota mediated by microbe-derived indole metabolites.

Keywords: *Lacticaseibacillus rhamnosus*; *Salmonella* infection; intestinal dysbacteriosis; tryptophan metabolism; indole-3 acrylic acid; pro-inflammatory response

Introduction

Diarrhoeal diseases caused by infectious agents (e.g., pathogens and parasites) remain a severe health burden worldwide. Approximately 1.7 billion childhood diarrhoea cases are recorded annually, with diarrhea responsible for over 480 thousand deaths for children aged <5 years and over 500 thousand deaths for adults aged >70 years each year (Thiagarajah et al., 2015; UNICEF, 2022; WHO, 2017). As one of the most common foodborne enteric pathogens, *Salmonella* infection leads to substantial gastroenteritis incidents, imposing enormous economic burdens on global society and posing disproportionate threats to animal and human health (Kim and Isaacson, 2017; Stanaway et al., 2019). *Salmonella* has evolved strategies to subvert colonization resistance conferred by intestinal commensals and evade host immune defense responses, contributing to the increasing incidence of Salmonellosis (Caballero-Flores et al., 2022; Fu et al., 2019). *Salmonella*-contaminated food (meat, eggs, dairy) is considered the leading cause of Salmonellosis, estimated to cause a total global

economic loss of over $3.5 billion annually in the US (Kim and Isaacson, 2017). Traditionally, antibiotic treatment has been the primary strategy to control *Salmonella* infectious diseases (Eng et al., 2015). However, the global abuse of antibiotics has raised significant concerns about antimicrobial resistance (AMR), foodborne antibiotic residues, and compromises in treating antimicrobial resistant bacterial infections (Fishbein et al., 2023; Olesen et al., 2018). These issues have inspired interest in seeking alternative strategies, such as dietary interventions (e.g., probiotics, prebiotics, natural products), to prevent *Salmonella* infectious disease outbreaks.

Microbial dysbiosis induced by antimicrobials, enteric infections, and irregular dietary habits increases the susceptibility to pathogen infection and other diseases, such as inflammatory bowel disease (Gillis et al., 2018b; Levy et al., 2017). Therefore, a balanced intestinal microbiota and metabolic functions are crucial for maintaining gastrointestinal homeostasis. Gut commensal microbes and their derivatives have been proven to exhibit broad antimicrobial activities and protect the host against pathogen infections by providing colonization resistance against enteric pathogens, limiting pathogen colonization, invasion and transmission, and maintaining intestinal barrier function (Caballero-Flores et al., 2023; Jacobson et al., 2018; Wan et al., 2019). As one of the intestinal commensal microbes, probiotic species (without residues in raw food products), such as *Lactobacillus*, *Bifidobacterium*, *Bacillus* and yeast (e.g., *Saccharomyces boulardii*, *S. cerevisiae*), exert beneficial effects on the host by enhancing colonization resistance and immune defense, inhibiting colonization and invasion against pathogens, and maintaining gastrointestinal homeostasis (Gareau et al.,

2010; Xiao et al., 2021). Although many candidate probiotic isolates have been uncovered from fermented foods and mammalian intestines (Sakandar and Zhang, 2021; Wang et al., 2022), the traditional strategies for screening these candidates are both time-consuming and labor-intensive, involving bacterial isolation, culturing, phenotypic characterization, randomized controlled trials, and various *in vitro* and *in vivo* tests to assess probiotic properties (Sun et al., 2022). While culture-dependent methods are classic strategies, emerging evaluation strategies for candidates, such as whole-genome sequencing-based approaches and small invertebrate models (e.g., *C. elegans*, *Drosophila*), have gained significant attention due to their high-throughput, replicable and standardized properties (Sun et al., 2022; Wang et al., 2022).

Intestinal macrophages play vital roles in maintaining gut homeostasis, regulating inflammation, and particularly in promoting the resolution of inflammation (Lavelle and Sokol, 2020; Na et al., 2019), which has been considered as a novel potential target for controlling intestinal pro-inflammatory disorders. It has been reported that probiotics-derived metabolites, such as bacteriocins, antimicrobial compounds, short-chain fatty acids, and tryptophan/indole derivatives, can mediate the beneficial effects of probiotics on the host health by interacting with the host gastrointestinal immune cells and gut residents (Britton and Faith, 2021; Sanders et al., 2019). Bacterial tryptophan metabolism produces indole derivatives (e.g., indole-3-acetic acid, 3-indolepropionic acid, 3-indoleacrylic acid, indole-3-lactic acid, indole-3-aldehyde, indole-3-acetaldehyde), which are potent bioactive ligands for the aryl hydrocarbon receptor (AHR) (Agus et al., 2018; Koh and Backhed, 2020). These indole derivatives

111 play crucial roles in maintaining gut barrier integrity and homeostasis by activating
112 AHR signaling pathway (Agus et al., 2018). *Limosilactobacillus reuteri*-produced
113 indole derivatives have been reported to exert anti-inflammatory effects by activating
114 AHR signaling pathway (Cervantes-Barragan et al., 2017). Although the beneficial
115 effects of probiotics in protecting the host against diverse enteric infections have been
116 extensively examined, the interactive roles between pro-inflammatory macrophages
117 and microbe-tryptophan/indole metabolites in combating enteric infections have not
118 been fully studied yet. Here, we found that *Lacticaseibacillus rhamnosus* P118 exerts
119 great probiotic properties after assessing by traditional and C. elegans-infection
120 screening strategies. P118 exhibited broad antibacterial activities and reduced host
121 susceptibility to enteric *Salmonella* infection by improving intestinal dysbiosis and
122 fecal metabolite changes, and inhibiting intestinal pro-inflammatory responses.
123 Integrated omics further demonstrated that P118 probiotic activities in enhancing host
124 tolerance to *Salmonella* infection were mediated by microbe-derived tryptophan/indole
125 metabolites.
126

127 **Results**

128 **Two screening approaches to convergent probiotic candidates**

129 After identified by MALDI-TOF MS, a total of 290 bacterial isolates were isolated and
130 identified from 33 fermented yoghurts samples and 6 healthy piglet rectal content
131 samples. Those isolates consist of 63 *Streptococcus* isolates, 158
132 *Lactobacillus/Lacticaseibacillus*/*Limosilactobacillus* isolates, and 69 *Enterococcus*

133 isolates (Figure 1A, Table 1). Two screening strategies were employed in the present
134 study to further investigate the potential probiotic properties of the isolates: the
135 traditional/classic approach and the *C. elegans* infection approach. In the
136 traditional/classic approach, 27 isolates were screened out by milk-clotting activity
137 assay (Figure 1A, Table S1), among which two isolates (P118 and P199) exhibited the
138 highest tolerance to bile salt (0.3%~2.0%) (Figure 1B) and biofilm formation
139 capabilities (Figure 1C). Compared with the P199 strain, P118 strain exhibited the
140 highest susceptibility to multiple antimicrobials (Figure S1A). *C. elegans* has been
141 widely used as an invaluable model for understanding the conserved mechanisms of
142 host-microbe interactions, due to the similarities of gut morphology and physiological
143 function with human and animal (Kumar et al., 2020). In the *C. elegans* infection
144 approach, 8 out of 290 isolates significantly increased the survivals and prolonged the
145 life span of *S*. Typhimurium-infected *C. elegans* ($P < 0.05$), and three isolates (P118,
146 P119, P120) treated worms were more resistant to *S*. Typhimurium infection than the
147 other isolates ($P < 0.05$) (Figure 1D, Table S2). Integrating the results of both screening
148 approaches, *L. rhamnosus* P118 strain exhibits versatile capabilities as a probiotic
149 candidate (Figure 1E).
150 To illustrate the probiotic properties of *L. rhamnosus* P118, antibacterial activity
151 evaluation *in vitro* was further conducted, and the results showed that the fermented
152 supernatants of P118 significantly inhibited the growth of multiple pathogens (e.g.,
153 *Salmonella*, *Yersinia*, *S. aureus*, *E. coli*, *C. rodentium*, *P. aeruginosa*, *R. anatipestifer*)
154 (Figure S1B). Interestingly, the inhibitory effect of P118 against *S*. Typhimurium was

155 in dose- and oxygen-dependent manners and results showed that high-dose and
156 anaerobic cultures exhibited more antibacterial effects than low-dose and aerobic
157 cultures, respectively ($P < 0.05$) (Figure 1F). Active factors derived from P118 to exert
158 antibacterial effects were explored. The results showed that the antibacterial activities
159 of the fermented supernatant (pH = 3.4) were sensitive to alkalinity (pH > 5.0), trypsin,
160 proteinase-K, pepsin and high temperature (> 70°C), but were resistant to catalase
161 treatment (Figure 1G-H). The fermented cultures and supernatants of P118 not only
162 significantly inhibited the growth of *S*. Typhimurium *in vitro* (Figure 1I), but also
163 protected worms against *S*. Typhimurium infection (Figure 1G, Table S3). Although
164 they exhibited no antibacterial activities *in vitro* (Figure 1I), the protective activities of
165 heat treated P118 and P118 lysates against *S*. Typhimurium pathogenesis were observed
166 in *C. elegans* but weaker than that of the fermented cultures and supernatants (Figure
167 1G).

168 **P118 genomics analysis suggests genetic determinants for antibacterial actions**

169 Subsequently, whole genome sequencing of P118 was performed to explore the
170 potential antibacterial factors based on genomic evidence. The results showed that
171 species-level identity for P118 isolate with 2.99 Mb genome size was confirmed at $P <$
172 0.0001 (Figure S2A, Figure 1K, Table S4), and P118 draft genome was most closely
173 related to *L. rhamnosus* subspecies (NCTC13710 and BIO5326) (Figure 1K, Table S5,
174 Figure S2B). Genomic analysis using antiSMASH and BAGEL4 databases revealed the
175 presence of putative bacteriocin synthesis genes in P118 isolate (Figure 1L). Putative
176 bacteriocins predicated in P118 isolate showed high homology with known class II

177 bacteriocins (IIa carnobacteriocin B2 produced by *C. maltaromaticum*, IIb enterocin X
178 produced by *Enterococcus faecium* KU-B5, IId/b lactococcin A/G, and some novel
179 bacteriocin-encoded hypothetical proteins). Collective data demonstrates that *L.*
180 *rhamnosus* P118 exhibits outstanding probiotic traits.

181 **P118 protects lethal *S*. Typhimurium infections in a murine model**

182 The protective activity of *L. rhamnosus* P118 against enteric pathogens was further
183 examined in the *Salmonella*-infected murine model (Figure 2A). Administration of
184 P118 significantly protected mice against *Salmonella*-induced deaths and body weight
185 losses (Figure 2B-C), accompanied by the alleviated splenomegaly, hepatomegaly,
186 shortened gastrointestinal tract and clinical and pathological score (Figure 2D-F, Figure
187 S3B). Meanwhile, P118 significantly limited *Salmonella* colonization in the intestinal
188 tissues (duodenum and colon) and invasion into the peripheral organs (liver and spleen)
189 of mice, thereby markedly reducing *Salmonella* fecal shedding (Figure 2G).
190 Additionally, *Salmonella* infection-induced ileal mucosal damage was alleviated by
191 P118 administration, as illustrated by the increased ileal villus height (Figure 2H, Figure
192 S3C), ratio of villus height/crypt-depth (Figure 2H, Figure S3D), ileal microvilli height
193 and density (Figure 2H, Figure S3E-F), the upregulated ZO-1 mRNA expression
194 (Figure S4A), and the downregulated *IL-1β* mRNA expression (Figure S4E),
195 accompanied by the reduced IL-1β level in serum (Figure S4D). Intervention with P118
196 significantly increased the numbers of Ki67-positive cells (proliferating cells), Muc2-
197 positive cells (goblet cells), and decreased the numbers of F4/80-positive cells
198 (macrophages) and F4/80^{+} iNOS^{+} cells (pro-inflammatory macrophages) in the ileum

199 (Figure 2H) and also attenuated the pathological damages of peripheral organs (liver
200 and spleen) caused by *Salmonella* infection (Figure S3A & B).

201 **P118 improves *Salmonella* infection by modulating gut microbiota**

202 Gut microbes play crucial roles in host physiological activities, and colonization
203 resistance against enteric pathogens (Jacobson et al., 2018), and dysbiosis is supposedly
204 associated with *Salmonella* infection (Gillis et al., 2018a). Significant bacterial
205 community structures among four groups were observed (Figure 3A, Table S8), and
206 most of the bacterial operational taxonomic units (OTUs) were classified as group-
207 specific OTUs (Figure 3B). Compared to the uninfected group, *Salmonella* infection
208 significantly depleted 167 OTUs and enriched 60 OTUs (Figure 3C), whereas
209 compared to the *Salmonella*-infected group, pretreatment with P118 significantly
210 depleted 16 OTUs and enriched 52 OTUs (Figure 3D). Specifically, *Salmonella*
211 infection significantly increased the relative abundances of potentially harmful
212 microbes (e.g., *Salmonella*, *Escherichia*-Shigella, *Klebsiella*, *Morganella*,
213 *Akkermansia*) and significantly reduced the relative abundances of SCFA-producing
214 and potentially beneficial microbes (e.g., *Alloprevotella*, *Lactococcus*,
215 *Faecalibacterium*, *Limosilactobacillus*, *Parasutterella*, *Odoribacter*, *Dubosiella*,
216 *Candidatus arthromitus*) (Figure 3E, Figure S5B). Pretreatment with P118 significantly
217 reduced the relative abundances of pathogenic microbes (e.g., *Salmonella*,
218 *Anaeroplasma*, *Klebsiella*, *Morganella*) and significantly increased the relative
219 abundances of potentially beneficial or commensal microbes (e.g.,
220 *Candidatus_Saccharimonas*, *Turicibacter*, *Enterorhabdus*) (Figure 3F, Figure S5C).

221 Based on the changes in bacterial community structures, the internal driving forces of
222 gut microbial communities were investigated using ecological models. Both null model
223 and neutral community model analyses revealed that the stochastic processes belonging
224 to homogenizing dispersal exerted important roles in *Salmonella*-infected mice gut
225 microbiome assembly, whereas the deterministic processes (homogeneous selection
226 and variable selection) exerted more influences on P118-pretreated mice gut
227 microbiome assembly than *Salmonella*-infected mice (Figure S6A-B).

228 **Microbe-derived tryptophan metabolites are associated with the protection**

229 Significant differences in fecal metabolite structures among the three groups separated
230 into distinct clusters were also observed (Figure 4A, Table S9). Compared with the
231 uninfected group, *Salmonella* infection significantly upregulated 256 fecal metabolites
232 ($\log_2$(fold change) > 1, $P < 0.05$) and downregulated 402 fecal metabolites ($\log_2$(fold
233 change) < 1, $P < 0.05$) (Figure 4B), and pretreatment with P118 significantly enriched
234 100 metabolites ($\log_2$(fold change) > 1, $P < 0.05$) and depleted 81 metabolites ($\log_2$(fold
235 change) < 1, $P < 0.05$) (Figure 4C). Among the significant differential metabolites, 91
236 metabolites (VIP > 1) downregulated in *Salmonella*-infected mice were upregulated
237 explicitly in P118-pretreated mice (Figure S7A&C, Table S10), and 43 metabolites
238 (VIP > 1) upregulated in *Salmonella*-infected mice were downregulated explicitly in
239 P118-pretreated mice (Figure S7B&C, Table S10). KEGG pathway analysis revealed
240 that fecal metabolites were mainly enriched in tryptophan metabolism, fatty acid
241 biosynthesis, biosynthesis of amino acids and neuroactive ligand-receptor interaction
242 pathways in P118-pretreated mice (Figure 4D). Interestingly, pretreatment with P118

243 significantly increased the fecal levels of tryptophan and tryptophan derivatives (indole,
244 indole-3-acrylic acid, 5-hydroxytryptophan, 5-methoxyindoleacetate) (Figure 4E).
245 Pearson correlation analysis showed that *S.* Typhimurium burdens (in the duodenum,
246 colon, liver, spleen, feces) and organ (spleen, liver) indices were negatively correlated
247 with the levels of fecal tryptophan and tryptophan derivatives (indole, indole-3-acrylic
248 acid, 5-hydroxytryptophan, protocatechuic acid, trans-cinnamaldehyde, 5-
249 methoxyindole-3-carbaldehyde) and positively correlated with the levels of (serotonin,
250 tryptophanol, 3-(2-hydroxyethyl) indole, tryptamine) (Figure 4F). Conversely, the body
251 weight was positively correlated with the levels of fecal tryptophan and tryptophan
252 derivatives (Figure 4F). Bio-Sankey network analysis further showed that 26 genera
253 were identified as potential bacteria that might participate in the metabolic reaction
254 R02340 (tryptophan synthase, indoleglycerol phosphate and indole), of which five
255 bacteria (*Bifidobacterium*, *Lacticaseibacillus*, *Enterococcus*, *Staphylococcus*, and
256 *Pseudomonas*, dark red if $P < 0.05$) were positively associated with indole in the
257 metabolic reaction R02340 (Figure 4G). These results indicate that microbe-derived
258 tryptophan metabolites are associated with P118-mediated protection against
259 *Salmonella* infection.
260 Based on the findings above that *Lacticaseibacillus* species were involved in
261 tryptophan biosynthesis and metabolism, *L. rhamnosus* P118 genome was reanalyzed
262 to determine whether P118 encode enzymes necessary to exert this function. The
263 genomic data further showed that P118 encoded various genes (e.g., *fldH*, *AraT*, *AspB-*
264 *4*, *AmiE*, *trpA*, *trpB*, *BCAT*, *IGPS*, *MT*) essential to biosynthesize and metabolize

265 tryptophan into tryptophan derivatives (Figure 4H, Table S11). The metabolomic results
266 of P118 cultures also validated the genomic data that P118 could secrete a diverse
267 profile of tryptophan-derived metabolites (e.g indole-3-acrylic acid, indole, indole-3-
268 lactic acid, DL-tryptophan, kynurenine, N-Acetyl-D-tryptophan, 5-
269 methoxyindoleacetic acid, 5-hydroxytryptophan) (Table S12). Taken together, these
270 data suggest that P118-derived tryptophan metabolites might contribute to the
271 protection against *Salmonella* infection.

272 **Indole-3-acrylic acid protects against *Salmonella* infection by inhibiting**
273 **macrophage pro-inflammatory responses**

274 Based on the above results, exogenous indole-3-acrylic acid (IAA) was employed to
275 further explore its roles against *Salmonella* infection. The antibacterial assay results
276 showed that IAA (> 4.4 mM) significantly inhibited *Salmonella* growth (Figure S8).
277 Exogenous IAA administration significantly reduced mice susceptibility to *Salmonella*
278 infection， as evidenced by the increased body weight (Figure 5B), the alleviated
279 splenomegaly and hepatomegaly (Figure 5D, 5F), and the increased colon length
280 (Figure 5C). Meanwhile, IAA administration significantly inhibited *Salmonella*
281 colonization in the intestinal tissues (cecum and colon) and invasion into the peripheral
282 organs (liver and spleen) of mice, thereby markedly reducing *Salmonella* fecal shedding
283 (Figure 5E). Additionally, *Salmonella* infection-induced ileal mucosa damage was
284 alleviated by exogenous IAA, as illustrated by the increased ileal villus height (Figure
285 5G, 5I), and the increased numbers of Muc2-positive goblet cells in the ileum (Figure
286 5H, 5I). Exogenous IAA intervention significantly reduced *Salmonella* infection-

287 induced intestinal pro-inflammatory responses, as evidenced by the decreased numbers
288 of F4/80-positive macrophages (Figure 5I), the downregulated mRNA (*IL-1β*, *IL-6*, *IL-*
289 *18*, *TNF-α*, *iNOS*) expression (Figure 5H), and the reduced protein (iNOS, IL-1β, IL-6,
290 TNF-α, markers of pro-inflammatory macrophages) expression (Figure 5I).
291 The *in vitro* experiments further showed that, although failed to increase the uptake of
292 *Salmonella* (Figure S9A, 0h), IAA treatment significantly reduced intracellular
293 *Salmonella* survival in RAW 264.7 macrophage cells (Figure S9A, 6h, 12h), which
294 could be reversed by pretreatment with AHR inhibitor CH-223191 (Figure S9A, 6h,
295 12h), indicating that IAA enhances the intracellular bactericidal capacity of RAW 264.7
296 cells. Furthermore, IAA treatment significantly inhibited *Salmonella* infection-induced
297 pro-inflammatory responses, as evidenced by inhibiting mRNA (*IL-1β*, *IL-6*, *IL-18*,
298 *TNF-α*, *iNOS*) expression and nitric oxide secretion of *Salmonella*-infected RAW 264.7
299 macrophage cells, which blocked by the presence of AHR inhibitor CH-223191 (Figure
300 S9B-G).
301 Macrophages play important roles in initiating immune responses, maintaining gut
302 homeostasis and phagocytic clearance of pathogens (Na et al., 2019). To further
303 investigate the involved roles of macrophages in P118/IAA-mediated protective effect,
304 *in vivo* macrophage depletion using clodronate liposomes was conducted. As expected,
305 macrophage depletion significantly blocked the protection of P118 and exogenous IAA
306 against *Salmonella* infection (Figure 6A-I). P118 or exogenous IAA administration
307 failed to increase the body weight (Figure 6B) and colon length (Figure 6E), alleviate
308 the splenomegaly and hepatomegaly (Figure 6C, 6D), inhibit the colonization, invasion

309 and shedding of *Salmonella* (Figure 6F) after the intestinal macrophage depletion.
310 Additionally, after depleting the intestinal macrophage, P118 or exogenous IAA
311 administration also failed to attenuate *Salmonella* infection-induced intestinal mucosa
312 damage (Figure 6G, 6H, 6I) and pro-inflammatory responses (Figure 6H, 6I). Taken
313 together, these findings indicate that P118 and IAA protect against *Salmonella* infection
314 by inhibiting pro-inflammatory responses of intestinal macrophage.
315

316 **Discussion**

317 Fermented foods and mammalian intestines are rich in lactic acid bacteria that can
318 produce organic acids and lactobacillin to inhibit overgrowth, adhesion, invasion and
319 toxin secretion of pathogens (Gareau et al., 2010; Wan et al., 2019). Traditionally, the
320 culturomics strategy, together with multiple evaluation assays, is the primary way to
321 search potential probiotic species from the complex microbial community, which is
322 both time- and labor-consuming (Wang et al., 2022). Although the whole genomic
323 sequencing-based approach is an emerging favorable way to screen potential probiotic
324 strains, it's hard to widely adopt based on numerous isolates due to the high sequencing
325 costs (Schwarze et al., 2020). Given that the similarities of gut morphology and
326 physiological function with human and animal, *C. elegans* provides an invaluable
327 model to investigate host-microbe interactions and probiotic properties of beneficial
328 microbes at low cost (Kumar et al., 2020; Poupet et al., 2020). In the present study, we
329 found *Salmonella* infection significantly induced death and decreased the lifespan of *C.*
330 *elegans*, indicating *C. elegans* is very susceptible to *S.* Typhimurium infection,

331 consistent with a previous report (Rangan et al., 2016). Integrating the results of
332 culturomics and *C. elegans* infection strategies, *L. rhamnosus* P118 with excellent
333 probiotic properties was screened from 290 isolates and exhibited broad *in vitro*
334 antibacterial activities. Interestingly, high fermented dose and anaerobic cultures of
335 P118 showed more antibacterial effects than low dose and aerobic cultures, indicating
336 that the active factors were more released by P118 at the stationary phase under
337 anaerobic conditions. What's more, the antibacterial activities of the fermented
338 supernatant were sensitive to alkalinity, trypsin, proteinase-K, pepsin, and high
339 temperature, indicating that the active secreted factors in the fermented supernatant
340 were protein- or peptide-based active agents, consistent with a previous report that *L.*
341 *rhamnosus* exerted antibacterial effects by secreting bioactive peptides (Iram et al.,
342 2022). Although limited studies have reported bacteriocin-like activity in *L. rhamnosus*,
343 it remains unclear whether this species produces active bacteriocins (Kankainen et al.,
344 2009). Nonetheless, genomic data in this study revealed the presence of putative
345 bacteriocin synthesis genes in P118 genome. In agreement with a previous study
346 (Kankainen et al., 2009), the predicated bacteriocins showed high homology with
347 known class II bacteriocins (e.g., IIa carnobacteriocin B2 produced by *C.*
348 *maltaromaticum*, IIb enterocin X produced by *Enterococcus faecium* KU-B5), which
349 needs to be further validated by gene-editing technology and synthetic biology.
350
351 To further validate the antibacterial activities of *L. rhamnosus* P118 against enteric
352 pathogens, *Salmonella*-infected mice model was employed. We found that

353 administration of P118 significantly reduced mice susceptibility to *S.* Typhimurium
354 infection by improving intestinal health, dysbiosis and the changes of fecal metabolite
355 profiles. Colonized *S.* Typhimurium in the intestine disrupts structural and functional
356 intestinal integrity, leading to substantial immune response and severe epithelial barrier
357 damage, and then migrates to internal organs (liver, spleen) via the blood circulatory
358 system, causing splenomegaly and hepatomegaly (Rogers et al., 2022; Wang et al.,
359 2021a). In the present study, P118 significantly increased *Salmonella*-infected mice
360 survival and alleviated *Salmonella*-induced splenomegaly and hepatomegaly. The
361 beneficial attenuated effect was partly contributed by the reduced *Salmonella*
362 colonization in intestine and invasion into the peripheral organs, and eventually, the
363 decreased fecal shedding, consistent with previous reports (Liu et al., 2023; Wu et al.,
364 2024). It's reported that *S.* Typhimurium exploits and disrupts intestinal barrier integrity
365 to adhere, and disseminate deeper into intestinal mucosa, and evade immune clearance
366 (Bernal-Bayard and Ramos-Morales, 2018; Hiyoshi et al., 2022). In the current study,
367 P118 treatment also significantly improved the structural and functional intestinal
368 integrity, attenuated inflammatory responses, reduced the numbers of F4/80-positive
369 macrophages and proinflammatory macrophages ($F4/80^+$ $iNOS^+$ cells), and increased
370 the numbers of Ki67-positive and Muc2-positive goblet cell in the ileum, demonstrating
371 that P118 improved the intestinal health and reducing pro-inflammatory responses of
372 intestinal macrophages, which further confirms the beneficial alleviated effect exerted
373 by *L. rhamnosus* P118.
374

375 Intestinal microbes play essential roles in providing colonization resistance against
376 enteric pathogens and pathobionts, and limiting adhesion, invasion and transmission of
377 pathogens (Caballero-Flores et al., 2022; Jacobson et al., 2018). Microbial dysbiosis
378 and excessive immune responses induced by enteric pathogens can, in turn, aggravate
379 and exacerbate gut permeability and damage (Read et al., 2021; Rogers et al., 2022).
380 Many studies have reported that *Salmonella* infection was often accompanied by
381 microbial dysbiosis (Gillis et al., 2018b; Read et al., 2021; Wang et al., 2021a). The
382 current results found that *L. rhamnosus* P118 treatment significantly restored the
383 bacterial community structures in *Salmonella*-infected mice, and significantly reduced
384 the relative abundances of potentially harmful microbes (e.g., *Salmonella*, *Klebsiella*,
385 *Anaeroplasma*, *Morganella*), which belong to pathogens and pathobionts (Dong et al.,
386 2022; Galan, 2021; Laupland et al., 2022). Structure composition and assembly of
387 microbial communities are essential for ecosystem function (Shi et al., 2023; Xun et al.,
388 2019), and revealing the underlying mechanisms of microbial community assembly is
389 a major goal of microbial community ecology (Jiao et al., 2020; Stegen et al., 2012).
390 Generally, stochastic (e.g., dispersal events, ecological drift, random birth, death) and
391 deterministic (e.g., interspecies interactions (e.g., competition, facilitation, mutualisms
392 and predation), species traits, environmental factors) processes are two major
393 ecological processes that drive microbiome assembly (Stegen et al., 2012; Zhou and
394 Ning, 2017). Deterministic processes mainly involve non-random and niche-based
395 mechanisms with abiotic and biotic factors that influence microbial community
396 assembly (Vellend, 2010), whereas stochastic processes mainly reflect random changes

397 in the relative abundance of species (Jiao et al., 2020; Jiao et al., 2021). Although
398 important in shaping the diversities of microbial composition and functions, the relative
399 contribution of microbiome assembly processes varies with different habitats (Jiao et
400 al., 2020; Jiao et al., 2021). The present study revealed that the stochastic processes
401 played dominant roles in intestinal microbiome assembly in *Salmonella*-infected mice,
402 indicating random changes occurred in the relative abundance of species. Conversely,
403 the deterministic processes played more significant roles in driving intestinal microbial
404 community assembly in P118-pretreated mice than in *Salmonella*-infected mice,
405 indicating abiotic factors (e.g., dietary intervention) or biotic interactions (e.g.,
406 microbial competition, facilitation, mutualism, predation, host filtering) might
407 influence the microbial community.
408
409 Accumulating evidence revealed that gut microbes-derived metabolites (e.g., short-
410 chain fatty acids, tryptophan/indole-derived metabolites, bacteriocins, bile acid, natural
411 products) are crucial mediators in host physiological activities (Cani, 2019; Wlodarska
412 et al., 2017), and metabolic disorders are major risk factors for bacterial infections
413 (Olive and Sassetti, 2016). In this study, the results showed that *L. rhamnosus* P118
414 improved *Salmonella* infection-induced fecal metabolite changes. Interestingly, P118
415 significantly increased the fecal levels of tryptophan and its derivatives (indole, indole-
416 3-acrylic acid, 5-hydroxytryptophan), and those metabolites were negatively correlated
417 with *S.* Typhimurium burdens (in the duodenum, colon, liver, spleen, feces) and organ
418 (spleen, liver) indices, and positively correlated with the body weight of mice,

419 indicating that microbiota-derived tryptophan/indole metabolites play beneficial roles
420 in P118 mediated probiotic activities in enhancing host tolerance to *Salmonella*
421 infection. It's reported that through binding to the aryl hydrocarbon receptor (AHR) of
422 host, bacterial tryptophan derivatives act as triggers to stimulate immune responses and
423 gut hormones to exert anti-inflammatory activities, enhance intestinal epithelial barrier,
424 and promote gastrointestinal motility, which contributes to host gastrointestinal
425 homeostasis and health (Agus et al., 2018; Cani, 2019). Our genomic and metabolomic
426 data further revealed that P118 could produce a wide array of tryptophan-derived
427 metabolites owing to encoding a variety of enzyme genes necessary to metabolize
428 tryptophan into indole derivatives; consistently, some *Lactobacillus* species broadly
429 conserved enzyme encoding genes that are involved in tryptophan metabolism
430 (Montgomery et al., 2022). The above results indicate that *L. rhamnosus* P118- and
431 microbe-derived tryptophan/indole metabolites might play positive roles in P118-
432 mediated probiotic activities. Although significant increases in microbe-derived
433 tryptophan/indole metabolites were observed in P118-treated mice, and it was
434 established that P118 can metabolize tryptophan into indole derivatives, it remains to
435 be investigated whether the differential tryptophan/indole metabolites were directly
436 derived from P118 or from other microbes. To test the roles of differential
437 tryptophan/indole metabolites in P118-mediated beneficial effects, exogenous indole-
438 3-acrylic acid, which significantly and negatively correlated with *S.* Typhimurium
439 burdens and hepatosplenomegaly mentioned above, was employed to investigate its
440 protective effect against *Salmonella* infection. Interestingly, we found that indole-3-

441 acrylic acid administration significantly enhanced mice tolerance to *S*. Typhimurium
442 infection by improving intestinal health and attenuating pro-inflammatory responses of
443 intestinal macrophages. Furthermore, the *in vitro* results also provide that indole-3-
444 acrylic acid enhanced bactericidal capacity of RAW 264.7 cells and inhibited *S*.
445 Typhimurium-induced pro-inflammatory responses, consistent with a previous report
446 (Wlodarska et al., 2017). Taken together, these results demonstrate that *L. rhamnosus*
447 P118/microbe-derived indole-3-acrylic acid play beneficial roles in P118-mediated
448 probiotic activities.
449 Macrophages are important in initiating immune responses, maintaining intestinal
450 immune homeostasis, phagocytic clearance of pathogens, tissue repair, and host defense
451 (Na et al., 2019; Neurath, 2024). It's reported that macrophages with strong plasticity
452 could be polarized into pro-inflammatory (M1) phenotype or proresolving (M2)
453 phenotype (Na et al., 2019). M1 macrophage activation is crucial and necessary for
454 pathogen clearance (Na et al., 2019). However, exaggerated immune responses
455 triggered by M1 macrophage are detrimental to the host by inducing tissue damage and
456 cell deaths (Wang et al., 2020). The current study showed that both *L. rhamnosus* P118
457 and indole-3-acrylic acid significantly attenuated *S*. Typhimurium infection-induced
458 pro-inflammatory responses, indicating that pro-inflammatory macrophages might be
459 key targets for *L. rhamnosus* P118 exerting probiotic effect. This hypothesis was
460 confirmed by macrophage depletion experiments that the protective effects of *L.*
461 *rhamnosus* P118 and indole-3-acrylic acid against *Salmonella* infection were abrogated
462 after intestinal macrophage depletion. Taken together, these results indicate that *L.*

463 *rhamnosus* P118/microbe-derived indole metabolites enhance host tolerance to
464 *Salmonella* infection by reducing intestinal pro-inflammatory responses, which also
465 provides a potential alternative strategy for using probiotics and their derived
466 metabolites to treat intestinal inflammatory disorders such as inflammatory bowel
467 disease (Lavelle and Sokol, 2020; Neurath, 2024).

468 **Conclusion**

469 In summary, two distinctive approaches were used to screen the probiotic candidate,
470 and the P118 strain was underscored for beneficial effects on a murine infection model.
471 Further, bacterial genomic sequencing, gut microbiota and metabolomic analysis
472 pinpointed the microbe-derived tryptophan/indole could be the importance of P118
473 probiotic properties. Nevertheless, the newly found P118 could enhance host tolerance
474 to *Salmonella* infections via various pathways, including direct antibacterial actions,
475 inhibiting *Salmonella* colonization and invasion, attenuating pro-inflammatory
476 responses of intestinal macrophages, and modulating gut microbiota mediated by
477 microbe-derived indole metabolites (Figure 7). Further investigations are needed to
478 assess whether the mechanisms observed in P118 are strain-specific or broadly
479 applicable to other *L. rhamnosus* strains, or LAB species in general.

480 **Materials and methods**

481 **Bacterial isolation and culture**

482 Lactic acid bacteria (LAB) and *Enterococcus* strains were isolated from 39 samples: 33
483 fermented yoghurts samples (collected from families in multiple cities of China,
484 including Lanzhou, Urumqi, Guangzhou, Shenzhen, Shanghai, Hohhot, Nanjing,

485 Yangling, Dali, Zhengzhou, Shangqiu, Harbin, Kunming, Puer), and 6 healthy piglet
486 rectal content samples without pathogen infection and diarrhea in pig farm of Zhejiang
487 province (Table 1). Ten isolates were randomly selected from each sample. De Man-
488 Rogosa-Sharpe (MRS) with 2.0% $CaCO_3$ and Brain heart infusion (BHI) broths
489 (Huankai Microbial, Guangzhou, China) were used for bacteria isolation and
490 cultivation. Matrix-Assisted Laser Desorption Ionization-Time of Flight Mass
491 Spectrometry (MALDI-TOF MS, Bruker Daltonik GmbH, Bremen, Germany) method
492 was employed to identify of bacterial species with a confidence level ⩾ 90% (He et
493 al., 2022). *Lacticaseibacillus rhamnosus* P118 (P118) and *Salmonella enterica* serovar
494 Typhimurium SL1344 (STm) were cultured in MRS and Luria Broth (LB) medium at
495 37 °C overnight under aerobic conditions, separately. The final concentration of
496 bacterial isolates was constantly checked by the spreading plate method (Wang et al.,
497 2023). After being centrifugated at 4000× g for 15 min at 4 °C, the fermented
498 supernatant of *L. rhamnosus* P118 was collected by centrifugation at 4000× g for 15
499 min at 4 °C, and then filtered through a 0.22 μm membrane (Merck Millipore,
500 Burlington, MA, USA) kept at 4 °C for further use.

501 **Probiotic property evaluation of candidate isolates**

502 For milk-clotting activity analysis of probiotics (Zhang et al., 2023), overnight
503 fermented lactic acid bacteria isolates under logarithmic growth were added to test
504 tubes containing skim milk (10% skim milk with 10 mM $CaCl_2$) at 1:20 ratio (v/v) and
505 then incubated at 37 °C. The coagulating time, final pH value and acidity of milk were
506 measured during the curdling process.

507 The bile salt tolerance assay was conducted according to a previous report (Wang et al.,
508 2023). Briefly, the isolates under logarithmic growth were resuspended into fresh MRS
509 medium (1% v/v) containing different (wt/v, 0, 0.3%, 0.6%, 1.0%, 1.5%, 2.0%) porcine
510 bile (MACKLIN®, Shanghai, China) and then plated into 96-well plates, after
511 incubation for 24h at 37 °C, the absorbance at 620 nm was measured by a SpectraMax
512 M5 reader (Molecular Devices, Sunnyvale, CA, USA).
513 Biofilm-forming assay of the isolates was performed as described previously (Zhou et
514 al., 2023). Briefly, 200 μL overnight cultures (adjusted to 2×10^6 CFU/mL) were added
515 into 96-well flat-bottom plates. After incubation for 36h at 37 °C, the planktonic cells
516 were discarded. After being gently washed three times with sterile PBS, the adherent
517 cells were stained with 200 μL of 0.4% crystal violet for 15 min at room temperature
518 and then washed with sterile PBS three times again. Finally, 200 μL 75% ethanol was
519 added to dissolve the stained adherent cells for 15 min, and biofilm was quantified by
520 measuring the absorbance at 590 nm using a SpectraMax M5 reader.
521 For antimicrobial susceptibility test, twelve antimicrobial agents (penicillins (PG),
522 erythromycin (EM), lincomycin (LM), gentamicin (GM), doxycycline (DOX),
523 ceftriaxone (CTR), norfloxacin (NOR), azithromycin (AZM), fleroxacin (FLE),
524 vancomycin (VA), streptomycin (STR)) were employed to evaluate the antimicrobial
525 susceptibility of the candidate probiotics by utilizing the Kirby-Bauer disk diffusion
526 method (Hudzicki, 2009).
527 The agar diffusion method (Wang et al., 2023) was used to evaluate the antimicrobial
528 activity against multiple pathogens *in vitro*. Briefly, bacterial culture medium (LB, BHI)

529 containing 0.25% (v/v) different zoonotic pathogens under logarithmic growth was
530 poured into 10-cm plates (Corning, NY, USA), separately. Then, 200 μL of the
531 fermented sterile supernatant collected from the overnight cultured *L. rhamnosus* P118
532 was added into 8 mm agar wells created by Oxford cup. The bacteriostatic effect was
533 evaluated by the growth inhibition zone around the 8-mm agar wells after overnight
534 incubation at 37 °C.

535 ***Caenorhabditis elegans* infection**

536 *C. elegans* infection model was performed as previously described (Rangan et al., 2016).
537 *C. elegans* N2 (Bristol) were routinely raised on Nematode Growth Media (NGM)
538 feeding with *E. coli* OP50, and L4-stage worms were prepared according to the
539 description in WormBook (Girard et al., 2007). 200 μL of the isolated isolates (adjusted
540 to 5×10^8 CFU/mL using M9 medium) and *L. rhamnosus* P118-related substances (e.g.,
541 mixed cultures, fermented sterile supernatants, P118 lysate, dead P118) were poured
542 onto NGM in 24-well plates, separately, and dried at 22 °C for 4 h. L4-stage worms
543 were then transferred to the lawns of the poured NGM plates (30 worms/plate) with
544 three plates per group for 24h. Then, the treated worms were washed and transferred to
545 lawns of STm (1×10^8 CFU/lawn) on NGM plates for infection. Worm survival was
546 monitored at 24-hour intervals for sixteen days.

547 **Whole genome sequencing and data analysis**

548 Whole genome sequencing, quality control, assembly and annotation of *L. rhamnosus*
549 P118 was conducted according to our previous study (Zhou et al., 2023) using PacBio
550 Sequel platform and Illumina NovaSeq PE150 at Novogene (Novogene Co, Ltd.,

551 Beijing, China), and the P118 draft genome is available in the Sequence Read Archive
552 under accession number PRJNA848987. *L. rhamnosus* P118 assembly was queried
553 against the NCBI non-redundant prokaryotic genomes database using the Microbial
554 Genomes Atlas (MIGA) webserver (database update to 10/10/2023) (Rodriguez et al.,
555 2018). Taxonomic classification was inferred by the maximum average amino acid
556 identity (AAI) against all genomes in the database, with p-values estimated from the
557 distribution of all the reference genomes in NCBI's RefSeq at each taxonomic level as
558 a readout of classification probability. Average nucleotide identity (ANI) and AAI
559 tables of maximally the top-50 reference hits in the database were extracted and graphed
560 as x-y scatter plots to determine the nearest phylogenetic neighbors. To generate
561 phylogenic trees of isolates and MIGA-identified nearest phylogenetic neighbors, the
562 interfered proteome from PROKKA isolate annotations, or as publicly available in
563 NCBI for applicable reference genomes were uploaded to the ANI/AAI-Matrix
564 calculator (Rodriguez-R and Konstantinidis, 2016). The resulting phylogenetic tree
565 based on AAI was visualized using the interactive tree of life (iTOL) (Letunic and Bork,
566 2021).
567 *L. rhamnosus* P118 tryptophan-associated enzymes were identified as previously
568 described (including TNA, TMO, TrpD, ArAT, ALD, IPDC, FldH, and AmiE)
569 (Montgomery et al., 2022). Briefly, enzyme commission numbers, where available, or
570 alternatively enzyme names, were queried in PATRIC, PATRIC Global Family (PGF)
571 cross-genus identifiers were extracted and compiled for query within the *L. rhamnosus*
572 P118 genome. Protein sequences of *L. rhamnosus* P118 identified enzymes were

573 analyzed using InterProScan for additional functional prediction, and sequence
574 homology to the previously experimentally validated enzymes within other bacterial
575 species was determined using Blastp at 30% cross-genus identify and 90% identity
576 within each species.

577 ***S.* Typhimurium murine infection model**

578 Animal assays, specifically eighty 6-week-old female C57BL/6 mice (Slac Animal Inc.,
579 Shanghai, China), were conducted in the Laboratory Animal Center of Zhejiang
580 University under light-controlled (12h light/dark cycle), temperature-controlled (22 ±
581 2°C) and humidity-controlled (55 ± 5°C) conditions. Forty mice were randomly
582 selected for survival evaluation under *S*. Typhimurium infection, and the rest were used
583 for sample collection on day 3 post-infection (Figure 2A). The mice were randomly
584 divided into four groups (n = 10/group): Control group (C), *L. rhamnosus* P118 group
585 (P), *S*. Typhimurium-infected group (S), and *L. rhamnosus* P118 protective group (P+S).
586 Mice in the C and S groups were drinking sterile water every day, respectively. Mice
587 in the P and P+ST groups were orally administered with *L. rhamnosus* P118 (1×10^8
588 CFU/mouse) daily for seven days. After that, mice were orally ingested with *S.*
589 Typhimurium SL1344 (1×10^8 CFU/mouse) or sterile PBS. All mice were allowed free
590 access to water and food, and weighed every day. Mice were euthanized on day 3 post-
591 infection. Spleen and liver were weighted for organ index calculation according to the
592 formula: organ index = organ weight (g) / body weight (g) *1000.

593 To evaluate the protective effect of indole-3-acrylic acid (IAA), eighteen mice were
594 randomly divided into three groups (n = 6/group): Control group (C), *S*. Typhimurium-

595 infected group (S), and indole-3-acrylic acid protective group (IAA+S). Mice in the C
596 and S groups were drinking sterile water every day, respectively. IAA (Sigma, I3807)
597 was dissolved in 1 M NaOH in PBS and adjusted pH to 7.4 with 1 M HCl. Mice in the
598 IAA+ST groups were orally administered with 75mg/kg IAA daily for seven days. After
599 that, mice were orally ingested with *S.* Typhimurium SL1344 or sterile PBS. At 3 day-
600 post-infection, mice were euthanized for sample collection.

601 ***In vivo* macrophage depletion**

602 To evaluate the involved roles of macrophages, macrophage depletion assay was
603 conducted through intraperitoneal injection with 250 μL/mouse clodronate liposomes
604 (CLP, From Vrije Universiteit Amsterdam) twice (2 days prior and 1 day after
605 *Salmonella* infection, separately) according to the manufacturer's instructions. Thirty-
606 three mice were randomly divided into six groups (n = 3~6/group): Control group (C),
607 *S.* Typhimurium-infected group (S), Control group with macrophage depletion
608 (CLP+C), *S.* Typhimurium-infected group with macrophage depletion (CLP+S), IAA
609 protective group with macrophage depletion (CLP+IAA+S), and P118 protective group
610 with macrophage depletion (CLP+P+S). At 3 day-post-infection, mice were euthanized
611 for sample collection.

612 **Macrophage cell culture**

613 Murine macrophage cell line RAW 264.7 was cultured in DMEM/F12 medium (Gibco,
614 Carlsbad, CA) supplemented with 10% FBS (Gibco, CA) and 1% (v/v) antibiotic
615 solution (100 μg/mL streptomycin + 100 U/mL penicillin, Sigma-Aldrich, St. Louis,
616 MO) at 37°C in a 5% humidified CO_2 incubator. If not mentioned, the antibiotic

617 solution (100 μg/mL streptomycin and 100 U/mL penicillin) was not added into
618 DMEM/F12 medium in the further experiment.
619 For *S*. Typhimurium killing assay, RAW 264.7 cells seeded into 12-well plates (2 ×
620 10^6 cells/well) were treated with 100 μM IAA for 6h, followed by infecting with *S*.
621 Typhimurium (MOI = 10) for 1h. After washing 3 times with sterile PBS, the infected
622 RAW 264.7 cells were incubated for 0h, 6h and 12h in DMEM/F12 medium containing
623 gentamicin (50 μg/mL). At each time point, the infected RAW 264.7 cells were washed
624 with sterile PBS for 4 times and lysed with 0.01% Triton X-100 diluted in PBS. The
625 serial 10-fold dilutions of cell lysates were immediately plated on LB agar plates to
626 determine bacterial viability.
627 For the immune response assay, RAW 264.7 cells seeded into 12-well plates (2 × 10^6
628 cells/well) were pretreated with CH-223191 (AHR inhibitor, 10 μM) for 6h,
629 subsequently treating cells with 100 μM IAA for another 6h. After 6h, RAW 264.7 cells
630 were infected with *S*. Typhimurium (MOI = 10) for 2h. After washing 3 times with
631 sterile PBS, the infected RAW 264.7 cells were collected using RNAiso Plus (TaKaRa,
632 Dalian, China) for total RNA extracting and quantitative real-time PCR (qPCR). The
633 primer sets are listed in Table S6.

634 ***S*. Typhimurium burden**

635 *S*. Typhimurium loads in tissues (duodenum, cecum, colon, liver and spleen) and
636 shedding in feces were determined as previously described (Xu et al., 2018). Briefly,
637 tissues and fecal samples were collected under sterile conditions and homogenized in
638 sterile PBS containing 0.1% Triton X-100. Serial 10-fold dilutions of tissue

639 homogenates were spread onto SS agar plates in triplicate and then incubated at 37°C
640 overnight to quantify the bacterial colony-forming unit (CFU).

641 **Histopathology, immunofluorescent analysis, transmission electron microscope**
642 **(TEM) observation and clinical symptom score**

643 Tissues (ileum, liver and spleen) fixed in 4% paraformaldehyde were embedded in
644 paraffin, sliced, dehydrated and then sectioned for hematoxylin and eosin (H&E)
645 staining. The tissue slices were imaged and analyzed by using Olympus Microscope
646 (Tokyo, Japan). For the immunofluorescent assay, the paraffin-embedded ileum
647 samples were incubated with primary antibodies against Ki67 (GB121141, Servicebio,
648 China), lysozyme (GB11345, Servicebio, China), Muc2 (GB11344, Servicebio, China),
649 F4/80 (GB113373, Servicebio, China), iNOS (GB11119, Servicebio, China), IL-1β
650 (GB11113, Servicebio, China), IL-6 (GB11117, Servicebio, China), TNF-α (GB11188,
651 Servicebio, China) for overnight at 4°C and then further incubated with secondary
652 antibodies (Alexa Fluor® 488-conjugated goat anti-rabbit/mouse IgG) or HRP-
653 conjugated goat anti-rabbit secondary antibody (GB23303, Servicebio, China) for 60
654 min at room temperature. Finally, ileum slices were digitalized by Pannoramic MIDI
655 (3DHISTECH, Hungary).

656 TEM observations of ileum tissues were prepared according to our previous study
657 (Peng et al., 2022). Briefly, after being fixed with 2.5% buffered glutaraldehyde, ileum
658 segments were washed three times by cold 100-mM phosphate buffers, and then post-
659 fixed in 0.1% osmium tetroxide for 2 h, rapidly dehydrated in ascending grades of
660 ethanol (30, 50, 70, 95, and 100%), and moved into a 1:1 mixture of propylene oxide

661 and epoxy araldite. Finally, the ileum samples were observed and captured by the
662 transmission electron microscope (JEOL, Tokyo, Japan).
663 The clinical symptom scores were evaluated and graded by two blinded assessors
664 according to previous reported with modified (Burkholder et al., 2012), and the scoring
665 criteria are list in Table S7.

666 **ELISA assay and qPCR**

667 The serum contents of interleukin (IL)-1β and IL-18 were determined by ELISA kits
668 (Solarbio, Beijing, China) according to the manufacturer's instructions.
669 Total RNA extracted from intestinal tissues and RAW 264.7 cells by RNAiso Plus kit
670 (TAKARA, Dalian, China) was reverse-transcripted using PrimeScript II 1st Strand
671 cDNA Synthesis Kit (TAKARA, Dalian, China) according to the manufacturer's
672 instructions. The qPCR was then performed on the StepOne real-time PCR system
673 (Applied Biosystems) using SYBR PremixEx TaqII (TAKARA). The primer sets are
674 listed in Table S6. Fold changes were calculated after normalizing to the housekeeping
675 gene β-actin using the $2^{-\Delta\Delta Ct}$ method (Livak and Schmittgen, 2001).

676 **Microbiota analysis**

677 The TIANamp Stool DNA Kit (Tiangen, Beijing, China) was employed to extract fecal
678 bacterial genomic DNA, and fecal bacterial communities were investigated using 16S
679 rDNA sequencing by targeting the V3-V4 hypervariable region. The 16S rDNA
680 sequencing was then performed on an Illumina NovaSeq platform (Illumina Inc., San
681 Diego, CA, USA). The quality filter of the paired-end raw sequences and a cluster of
682 the filtered sequences into the operational taxonomic unit (OTU) at 97% similarity was

683 performed by QIIME software (version 1.9.1). Microbial OTU representative
684 sequences were assigned to a taxonomic lineage by the RDP classifier based on the
685 SILVA database (v 132 release).
686 To investigate the dissimilarities in bacterial communities and fecal metabolomes,
687 principal coordinates analysis (PCoA), analysis of similarities (ANOSIM),
688 permutational multivariate analysis of variance (PERMANOVA) and multi-response
689 permutation procedure (MRPP) were calculated using "vegan" package and visualized
690 using "ggplot2" package. Difference analysis of bacterial communities based on OUT
691 levels among groups was calculated using "DESeq2" package and was envisioned by
692 "UpSetR" and "ggplot2" packages. The significant differences in bacterial taxonomies
693 were analyzed and visualized by statistical analysis of taxonomic and functional
694 profiles (STAMP) software with a two-sided Welch's t-test (Parks et al., 2014).
695 The sloan neutral model was employed to estimate the importance of neutral processes
696 in the assembly of bacterial communities using "MicEco" package (Sloan et al., 2006).
697 A null-model-based statistical framework was conducted to evaluate the relative
698 importance of determinism and stochasticity in bacterial community assembly (Stegen
699 et al., 2013; Xu et al., 2022). Two assembly processes were defined as deterministic
700 processes ($|\beta NTI|>2$) and stochastic processes ($|\beta NTI|\leq 2$) based on the absolute values
701 of beta Nearest Taxon Index (βNTI) (Xu et al., 2020). Additionally, five ecological
702 assembly processes were then interpreted as homogeneous selection ($\beta NTI<-2$),
703 homogenizing dispersal ($|\beta NTI|\leq 2$ and $RC_{bray}<-0.95$), undominated ($|\beta NTI|\leq 2$ and
704 $|RC_{bray}|<0.95$), dispersal limitation ($|\beta NTI|\leq 2$ and $RC_{bray}>0.95$) and variable

705 (heterogeneous) selection (βNTI>2) based on the threshold of the absolute values of
706 βNTI and Bray-Curtis-based Raup-Crick (RC_{bray}) (Jiao et al., 2020; Xu et al., 2022).

707 **Metabolomics analysis**

708 Untargeted metabolomics was investigated to analyze the fecal metabolomes of mice.
709 The method for extracting metabolites from feces was conducted according to our
710 previous study described (Wang et al., 2021b). After extracting metabolites from feces,
711 UHPLC-MS/MS analyses of samples were performed by Vanquish UHPLC systems
712 (Thermo Fisher, Germany) coupled with Orbitrap Q Exactive™ HF-X mass
713 spectrometers (Thermo Fisher, Germany) in Novogene Co., Ltd. (Beijing, China).
714 Compound Discoverer 3.1 (CD3.1, Thermo Fisher) was employed to conduct peak
715 alignment, and quantify metabolites generated by UHPLC-MS/MS. After normalizing
716 to total spectral intensity and predicting molecular formula, the peaks were queried
717 against mzCloud, mzVault and MassList databases to extract the quantitative results.
718 Annotation of fecal metabolite signatures was queried against the KEGG database,
719 HMDB database and LIPIDMaps database. Significant differences in fecal metabolites
720 were analyzed using univariate analysis (t-test) and partial least-squares discriminant
721 analysis (PLS-DA), in which fecal metabolites with variable importance in the
722 projection (VIP) > 1 and $P < 0.05$ were considered differential metabolites. Pearson
723 correlation analysis between *S*. Typhimurium burden (in tissues and feces) and fecal
724 metabolites was analyzed and visualized using "linkET" package (Huang, 2021).
725 MetOrigin platform was employed to analyze the sources of microbial metabolites and
726 their metabolic functions in fecal metabolomes (Yu et al., 2022).

727 **Statistical Analysis**

728 The significance of the results was analyzed by one-way analysis of variance (ANOVA)
729 with Tukey's multiple comparisons test using SPSS v24 (SPSS Inc., Chicago, IL, USA)
730 and statistical graphs were visualized by GraphPad Prism v8.0 (GraphPad Software,
731 CA) and package "ggplot2" of R software (v4.3.1). * $P < 0.05$, ** $P < 0.01$, *** $P <$
732 0.001.

733

734 **Acknowledgements**

735 This work was supported by the National Program on Key Research Project of China
736 (2022YFC2604201) as well as the European Union's Horizon 2020 Research and
737 Innovation Programme under Grant Agreement No. 861917-SAFFI, Zhejiang
738 Provincial Key R&D Program of China (2023C03045, 2022C02024), Key Research
739 and Development Program of Hangzhou (202203A08), Zhejiang Provincial Natural
740 Science Foundation of China (LQ23C180005).

741 **Conflict of interest statement**

742 No potential conflict of interest was reported by the author(s).

743 **Data availability statement**

744 16S rRNA sequencing data is deposited at the Genome Sequence Archive (GSA) of the
745 BIG Data Center (https://bigd.big.ac.cn/gsa/) under accession no. PRJCA021751. *L.*
746 *rhamnosus* P118 isolate draft genome assembly is publicly available in the NCBI under
747 accession no. PRJNA848987.

748 **Ethics statement**

749 Animal procedures followed the guidelines and were approved by the Institutional
750 Animal Care and Use Committee of Zhejiang University (Permission number:
751 ZJU20220295).

752 **Author contributions**

753 Baikui Wang and Xianqi Peng: Investigation, Validation, Methodology, Data Analysis,
754 Visualization, Formal analysis, Writing - original draft & review & editing; Xiao Zhou,
755 Jiayun Yao, Haiqi Zhang, Weifen Li, Yan Li: Investigation, Writing – review; Min Yue:
756 Conceptualization, Resources, Methodology, Supervision, Writing – review & editing,
757 Funding acquisition, Project administration.

758 **References**

759 Agus A, Planchais J, Sokol H. Gut microbiota regulation of tryptophan metabolism in
760 health and disease. Cell Host Microbe 2018;23:716-24.
761 Bernal-Bayard J, Ramos-Morales F. Molecular mechanisms used by salmonella to
762 evade the immune system. Curr Issues Mol Biol 2018;25:133-68.
763 Britton GJ, Faith JJ. Causative microbes in host-microbiome interactions. Annu Rev
764 Microbiol 2021;75:223-42.
765 Burkholder T, Foltz C, Karlsson E, Linton CG, Smith JM. Health evaluation of
766 experimental laboratory mice. Curr Protoc Mouse Biol 2012;2:145-65.
767 Caballero-Flores G, Pickard JM, Nunez G. Microbiota-mediated colonization
768 resistance: Mechanisms and regulation. Nat Rev Microbiol 2022.
769 Caballero-Flores G, Pickard JM, Nunez G. Microbiota-mediated colonization
770 resistance: Mechanisms and regulation. Nat Rev Microbiol 2023;21:347-60.
771 Cani PD. Microbiota and metabolites in metabolic diseases. Nat Rev Endocrinol
772 2019;15:69-70.
773 Cervantes-Barragan L, Chai JN, Tianero MD, Di Luccia B, Ahern PP, Merriman J,
774 Cortez VS, Caparon MG, Donia MS, Gilfillan S, Cella M, Gordon JI, Hsieh CS,

775 Colonna M. Lactobacillus reuteri induces gut intraepithelial
776 cd4(+)cd8alphaalpha(+) t cells. Science 2017;357:806-10.
777 Dong N, Yang X, Chan EW, Zhang R, Chen S. Klebsiella species: Taxonomy,
778 hypervirulence and multidrug resistance. EBioMedicine 2022;79:103998.
779 Eng SK, Pusparajah P, Ab Mutalib NS, Ser HL, Chan KG, Lee LH. Salmonella: A
780 review on pathogenesis, epidemiology and antibiotic resistance. Frontiers in
781 Life Science 2015;8:284-93.
782 Fishbein SRS, Mahmud B, Dantas G. Antibiotic perturbations to the gut microbiome.
783 Nat Rev Microbiol 2023;21:772-88.
784 Fu A, Mo Q, Wu Y, Wang B, Liu R, Tang L, Zeng Z, Zhang X, Li W. Protective effect
785 of bacillus amyloliquefaciens against salmonella via polarizing macrophages to
786 m1 phenotype directly and to m2 depended on microbiota. Food & function
787 2019;10:7653-66.
788 Galan JE. Salmonella typhimurium and inflammation: A pathogen-centric affair. Nat
789 Rev Microbiol 2021;19:716-25.
790 Gareau MG, Sherman PM, Walker WA. Probiotics and the gut microbiota in intestinal
791 health and disease. Nat Rev Gastroenterol Hepatol 2010;7:503-14.
792 Gillis CC, Hughes ER, Spiga L, Winter MG, Zhu W, Furtado De Carvalho T, Chanin
793 RB, Behrendt CL, Hooper LV, Santos RL, Winter SE. Dysbiosis-associated
794 change in host metabolism generates lactate to support salmonella growth. Cell
795 Host Microbe 2018a;23:54-64 e6.
796 Gillis CC, Hughes ER, Spiga L, Winter MG, Zhu W, Furtado De Carvalho T, Chanin
797 RB, Behrendt CL, Hooper LV, Santos RL, Winter SE. Dysbiosis-associated
798 change in host metabolism generates lactate to support salmonella growth. Cell
799 Host Microbe 2018b;23:570.
800 Girard LR, Fiedler TJ, Harris TW, Carvalho F, Antoshechkin I, Han M, Sternberg PW,
801 Stein LD, Chalfie M. Wormbook: The online review of caenorhabditis elegans
802 biology. Nucleic Acids Res 2007;35:D472-5.
803 He D, Zeng W, Wang Y, Xing Y, Xiong K, Su N, Zhang C, Lu Y, Xing X. Isolation and
804 characterization of novel peptides from fermented products of lactobacillus for

805 ulcerative colitis prevention and treatment. Food Science and Human Wellness
806 2022;11:1464-74.
807 Hiyoshi H, English BC, Diaz-Ochoa VE, Wangdi T, Zhang LF, Sakaguchi M, Haneda
808 T, Tsolis RM, Baumler AJ. Virulence factors perforate the pathogen-containing
809 vacuole to signal efferocytosis. Cell Host Microbe 2022;30:163-70 e6.
810 Huang H. Linket: Everything is linkable. R package version 0.0.3 2021.
811 Hudzicki J. Kirby-bauer disk diffusion susceptibility test protocol. American society
812 for microbiology 2009;15:55-63.
813 Iram D, Kindarle UA, Sansi MS, Meena S, Puniya AK, Vij S. Peptidomics-based
814 identification of an antimicrobial peptide derived from goat milk fermented by
815 lactobacillus rhamnosus (c25). J Food Biochem 2022;46:e14450.
816 Jacobson A, Lam L, Rajendram M, Tamburini F, Honeycutt J, Pham T, Van Treuren W,
817 Pruss K, Stabler SR, Lugo K, Bouley DM, Vilches-Moure JG, Smith M,
818 Sonnenburg JL, Bhatt AS, Huang KC, Monack D. A gut commensal-produced
819 metabolite mediates colonization resistance to salmonella infection. Cell Host
820 Microbe 2018;24:296-307 e7.
821 Jiao S, Yang YF, Xu YQ, Zhang J, Lu YH. Balance between community assembly
822 processes mediates species coexistence in agricultural soil microbiomes across
823 eastern china. Isme Journal 2020;14:202-16.
824 Jiao S, Zhang B, Zhang G, Chen W, Wei G. Stochastic community assembly decreases
825 soil fungal richness in arid ecosystems. Mol Ecol 2021;30:4338-48.
826 Kankainen M, Paulin L, Tynkkynen S, Von Ossowski I, Reunanen J, Partanen P,
827 Satokari R, Vesterlund S, Hendrickx AP, Lebeer S, De Keersmaecker SC,
828 Vanderleyden J, Hamalainen T, Laukkanen S, Salovuori N, Ritari J, Alatalo E,
829 Korpela R, Mattila-Sandholm T, Lassig A, Hatakka K, Kinnunen KT,
830 Karjalainen H, Saxelin M, Laakso K, Surakka A, Palva A, Salusjarvi T, Auvinen
831 P, De Vos WM. Comparative genomic analysis of lactobacillus rhamnosus gg
832 reveals pili containing a human- mucus binding protein. Proc Natl Acad Sci U
833 S A 2009;106:17193-8.
834 Kim HB, Isaacson RE. Salmonella in swine: Microbiota interactions. Annual Review

835 of Animal Biosciences, Vol 5 2017;5:43-63.
836 Koh A, Backhed F. From association to causality: The role of the gut microbiota and its
837 functional products on host metabolism. Mol Cell 2020;78:584-96.
838 Kumar A, Baruah A, Tomioka M, Iino Y, Kalita MC, Khan M. Caenorhabditis elegans:
839 A model to understand host-microbe interactions. Cell Mol Life Sci
840 2020;77:1229-49.
841 Laupland KB, Paterson DL, Edwards F, Stewart AG, Harris PNA. Morganella morganii,
842 an emerging cause of bloodstream infections. Microbiol Spectr
843 2022;10:e0056922.
844 Lavelle A, Sokol H. Gut microbiota-derived metabolites as key actors in inflammatory
845 bowel disease. Nature Reviews Gastroenterology & Hepatology 2020;17:223-
846 37.
847 Letunic I, Bork P. Interactive tree of life (itol) v5: An online tool for phylogenetic tree
848 display and annotation. Nucleic acids research 2021;49:W293-W6.
849 Levy M, Kolodziejczyk AA, Thaiss CA, Elinav E. Dysbiosis and the immune system.
850 Nat Rev Immunol 2017;17:219-32.
851 Liu J, Liu H, Liu H, Teng Y, Qin N, Ren X, Xia X. Live and pasteurized akkermansia
852 muciniphila decrease susceptibility to salmonella typhimurium infection in
853 mice. J Adv Res 2023;52:89-102.
854 Livak KJ, Schmittgen TD. Analysis of relative gene expression data using real-time
855 quantitative pcr and the 2(t)(-delta delta c) method. Methods 2001;25:402-8.
856 Montgomery TL, Eckstrom K, Lile KH, Caldwell S, Heney ER, Lahue KG,
857 D'alessandro A, Wargo MJ, Krementsov DN. Lactobacillus reuteri tryptophan
858 metabolism promotes host susceptibility to cns autoimmunity. Microbiome
859 2022;10:198.
860 Na YR, Stakenborg M, Seok SH, Matteoli G. Macrophages in intestinal inflammation
861 and resolution: A potential therapeutic target in ibd. Nat Rev Gastroenterol
862 Hepatol 2019;16:531-43.
863 Neurath MF. Strategies for targeting cytokines in inflammatory bowel disease. Nat Rev
864 Immunol 2024.

865 Olesen SW, Barnett ML, Macfadden DR, Brownstein JS, Hernandez-Diaz S, Lipsitch
866 M, Grad YH. The distribution of antibiotic use and its association with antibiotic
867 resistance. Elife 2018;7.
868 Olive AJ, Sassetti CM. Metabolic crosstalk between host and pathogen: Sensing,
869 adapting and competing. Nature Reviews Microbiology 2016;14:221-34.
870 Parks DH, Tyson GW, Hugenholtz P, Beiko RG. Stamp: Statistical analysis of
871 taxonomic and functional profiles. Bioinformatics 2014;30:3123-4.
872 Peng X, Ed-Dra A, Song Y, Elbediwi M, Nambiar RB, Zhou X, Yue M.
873 Lacticaseibacillus rhamnosus alleviates intestinal inflammation and promotes
874 microbiota-mediated protection against salmonella fatal infections. Front
875 Immunol 2022;13:973224.
876 Poupet C, Chassard C, Nivoliez A, Bornes S. Caenorhabditis elegans, a host to
877 investigate the probiotic properties of beneficial microorganisms. Front Nutr
878 2020;7:135.
879 Rangan KJ, Pedicord VA, Wang YC, Kim B, Lu Y, Shaham S, Mucida D, Hang HC. A
880 secreted bacterial peptidoglycan hydrolase enhances tolerance to enteric
881 pathogens. Science 2016;353:1434-7.
882 Read E, Curtis MA, Neves JF. The role of oral bacteria in inflammatory bowel disease.
883 Nat Rev Gastroenterol Hepatol 2021;18:731-42.
884 Rodriguez-R LM, Konstantinidis KT, The enveomics collection: A toolbox for
885 specialized analyses of microbial genomes and metagenomes. PeerJ Preprints;
886 2016.p.
887 Rodriguez RL, Gunturu S, Harvey WT, Rossello-Mora R, Tiedje JM, Cole JR,
888 Konstantinidis KT. The microbial genomes atlas (miga) webserver: Taxonomic
889 and gene diversity analysis of archaea and bacteria at the whole genome level.
890 Nucleic Acids Res 2018;46:W282-W8.
891 Rogers AP, Mileto SJ, Lyras D. Impact of enteric bacterial infections at and beyond the
892 epithelial barrier. Nature Reviews Microbiology 2022.
893 Sakandar HA, Zhang HP. Trends in probiotic(s)-fermented milks and their in vivo
894 functionality: A review. Trends in Food Science & Technology 2021;110:55-65.

895 Sanders ME, Merenstein DJ, Reid G, Gibson GR, Rastall RA. Probiotics and prebiotics
896 in intestinal health and disease: From biology to the clinic. Nat Rev
897 Gastroenterol Hepatol 2019;16:605-16.
898 Schwarze K, Buchanan J, Fermont JM, Dreau H, Tilley MW, Taylor JM, Antoniou P,
899 Knight SJL, Camps C, Pentony MM, Kvikstad EM, Harris S, Popitsch N,
900 Pagnamenta AT, Schuh A, Taylor JC, Wordsworth S. The complete costs of
901 genome sequencing: A microcosting study in cancer and rare diseases from a
902 single center in the united kingdom. Genet Med 2020;22:85-94.
903 Shi J, Yang L, Liao Y, Li J, Jiao S, Shangguan Z, Deng L. Soil labile organic carbon
904 fractions mediate microbial community assembly processes during long-term
905 vegetation succession in a semiarid region. iMeta 2023:e142.
906 Sloan WT, Lunn M, Woodcock S, Head IM, Nee S, Curtis TP. Quantifying the roles of
907 immigration and chance in shaping prokaryote community structure. Environ
908 Microbiol 2006;8:732-40.
909 Stanaway JD, Parisi A, Sarkar K, Blacker BF, Reiner RC, Hay SI, Nixon MR, Dolecek
910 C, James SL, Mokdad AH, Abebe G, Ahmadian E, Alahdab F, Alemnew BT,
911 Alipour V, Bakeshei FA, Animut MD, Ansari F, Arabloo J, Asfaw ET,
912 Bagherzadeh M, Bassat Q, Belayneh YM, Carvalho F, Daryani A, Demeke FM,
913 Demis AB, Dubey M, Duken EE, Dunachie SJ, Eftekhari A, Fernandes E, Fard
914 RF, Gedefaw GA, Geta B, Gibney KB, Hasanzadeh A, Hoang CL, Kasaeian A,
915 Khater A, Kidanemariam ZT, Lakew AM, Malekzadeh R, Melese A, Mengistu
916 DT, Mestrovic T, Miazgowski B, Mohammad KA, Mohammadian M,
917 Mohammadian-Hafshejani A, Nguyen T, Nguyen H, Nguyen H, Nirayo YL,
918 Olagunju AT, Olagunju TO, Pourjafar H, Qorbani M, Rabiee M, Rabiee N,
919 Rafay A, Rezapour A, Samy AM, Sepanlou SG, Shaikh MA, Sharif M,
920 Shigematsu M, Tessema B, Tran BX, Ullah I, Yimer EM, Zaidi Z, Murray CJL,
921 Crump JA, Salm GN-T. The global burden of non-typhoidal salmonella invasive
922 disease: A systematic analysis for the global burden of disease study 2017.
923 Lancet Infectious Diseases 2019;19:1312-24.
924 Stegen JC, Lin X, Konopka AE, Fredrickson JK. Stochastic and deterministic assembly

925 processes in subsurface microbial communities. ISME J 2012;6:1653-64.
926 Stegen JC, Lin XJ, Fredrickson JK, Chen XY, Kennedy DW, Murray CJ, Rockhold ML,
927 Konopka A. Quantifying community assembly processes and identifying
928 features that impose them. Isme Journal 2013;7:2069-79.
929 Sun Y, Li HC, Zheng L, Li JZ, Hong Y, Liang PF, Kwok LY, Zuo YC, Zhang WY, Zhang
930 HP. Iprobiotics: A machine learning platform for rapid identification of
931 probiotic properties from whole-genome primary sequences. Briefings in
932 Bioinformatics 2022;23.
933 Thiagarajah JR, Donowitz M, Verkman AS. Secretory diarrhoea: Mechanisms and
934 emerging therapies. Nat Rev Gastroenterol Hepatol 2015;12:446-57.
935 Unicef, Diarrhoea remains a leading killer of young children, despite the availability of
936 a simple treatment solution. U Data (Ed.). https://data.unicef.org/topic/child-
937 health/diarrhoeal-disease/; 2022.p.
938 Vellend M. Conceptual synthesis in community ecology. Q Rev Biol 2010;85:183-206.
939 Wan MLY, Forsythe SJ, El-Nezami H. Probiotics interaction with foodborne pathogens:
940 A potential alternative to antibiotics and future challenges. Critical reviews in
941 food science and nutrition 2019;59:3320-33.
942 Wang B, Hussain A, Zhou Y, Zeng Z, Wang Q, Zou P, Gong L, Zhao P, Li W.
943 Saccharomyces boulardii attenuates inflammatory response induced by
944 clostridium perfringens via tlr4/tlr15-myd8 pathway in hd11 avian macrophages.
945 Poult Sci 2020;99:5356-65.
946 Wang B, Ye X, Zhou Y, Zhao P, Mao Y. Glycyrrhizin attenuates salmonella
947 typhimurium-induced tissue injury, inflammatory response, and intestinal
948 dysbiosis in c57bl/6 mice. Front Vet Sci 2021a;8:648698.
949 Wang B, Zhou Y, Mao Y, Gong L, Li X, Xu S, Wang F, Guo Q, Zhang H, Li W. Dietary
950 supplementation with lactobacillus plantarum ameliorates compromise of
951 growth performance by modulating short-chain fatty acids and intestinal
952 dysbiosis in broilers under clostridium perfringens challenge. Front Nutr
953 2021b;8:706148.
954 Wang B, Zhou Y, Wang Q, Xu S, Wang F, Yue M, Zeng Z, Li W. Lactiplantibacillus

955 plantarum lac16 attenuates enterohemorrhagic escherichia coli o157:H7
956 infection by inhibiting virulence traits and improving intestinal epithelial barrier
957 function. Cells 2023;12.
958 Wang L, Liu Q, Chen Y, Zheng X, Wang C, Qi Y, Dong Y, Xiao Y, Chen C, Chen T,
959 Huang Q, Zhai Z, Long C, Yang H, Li J, Wang L, Zhang G, Liao P, Liu YX,
960 Huang P, Huang J, Wang Q, Chu H, Yin J, Yin Y. Antioxidant potential of
961 pediococcus pentosaceus strains from the sow milk bacterial collection in
962 weaned piglets. Microbiome 2022;10:83.
963 Who, Diarrhoeal disease. 2017.p.
964 Wlodarska M, Luo C, Kolde R, D'hennezel E, Annand JW, Heim CE, Krastel P, Schmitt
965 EK, Omar AS, Creasey EA, Garner AL, Mohammadi S, O'connell DJ,
966 Abubucker S, Arthur TD, Franzosa EA, Huttenhower C, Murphy LO, Haiser HJ,
967 Vlamakis H, Porter JA, Xavier RJ. Indoleacrylic acid produced by commensal
968 peptostreptococcus species suppresses inflammation. Cell Host Microbe
969 2017;22:25-37 e6.
970 Wu Y, Zhang X, Liu X, Li Y, Han D, Pi Y, Whitmore MA, Lu X, Zhang G, Zheng J,
971 Wang J. Strain specificity of lactobacilli with promoted colonization by
972 galactooligosaccharides administration in protecting intestinal barriers during
973 salmonella infection. J Adv Res 2024;56:1-14.
974 Xiao Y, Zhai Q, Zhang H, Chen W, Hill C. Gut colonization mechanisms of
975 lactobacillus and bifidobacterium: An argument for personalized designs. Annu
976 Rev Food Sci Technol 2021;12:213-33.
977 Xu Q, Ling N, Chen H, Duan Y, Wang S, Shen Q, Vandenkoornhuyse P. Long-term
978 chemical-only fertilization induces a diversity decline and deep selection on the
979 soil bacteria. mSystems 2020;5.
980 Xu Q, Vandenkoornhuyse P, Li L, Guo J, Zhu C, Guo S, Ling N, Shen Q. Microbial
981 generalists and specialists differently contribute to the community diversity in
982 farmland soils. J Adv Res 2022;40:17-27.
983 Xu XG, Gong L, Wang BK, Wu YP, Wang Y, Mei XQ, Xu H, Tang L, Liu RR, Zeng
984 ZH, Mao YL, Li WF. Glycyrrhizin attenuates salmonella enterica serovar

typhimurium infection: New insights into its protective mechanism. Frontiers in Immunology 2018;9:2321.

Xun W, Li W, Xiong W, Ren Y, Liu Y, Miao Y, Xu Z, Zhang N, Shen Q, Zhang R. Diversity-triggered deterministic bacterial assembly constrains community functions. Nat Commun 2019;10:3833.

Yu G, Xu C, Zhang D, Ju F, Ni Y. Metorigin: Discriminating the origins of microbial metabolites for integrative analysis of the gut microbiome and metabolome. IMeta 2022;1:e10.

Zhang Y, Wang J, He J, Liu X, Sun J, Song X, Wu Y. Characteristics and application in cheese making of newly isolated milk-clotting enzyme from bacillus megaterium ly114. Food Res Int 2023;172:113202.

Zhou J, Ning D. Stochastic community assembly: Does it matter in microbial ecology? Microbiology and Molecular Biology Reviews 2017;81:e00002-17.

Zhou X, Kang X, Chen J, Song Y, Jia C, Teng L, Tang Y, Jiang Z, Peng X, Tao X. Genome degradation promotes salmonella pathoadaptation by remodeling fimbriae-mediated proinflammatory response. National Science Review 2023:nwad228.

1003 **Figures**

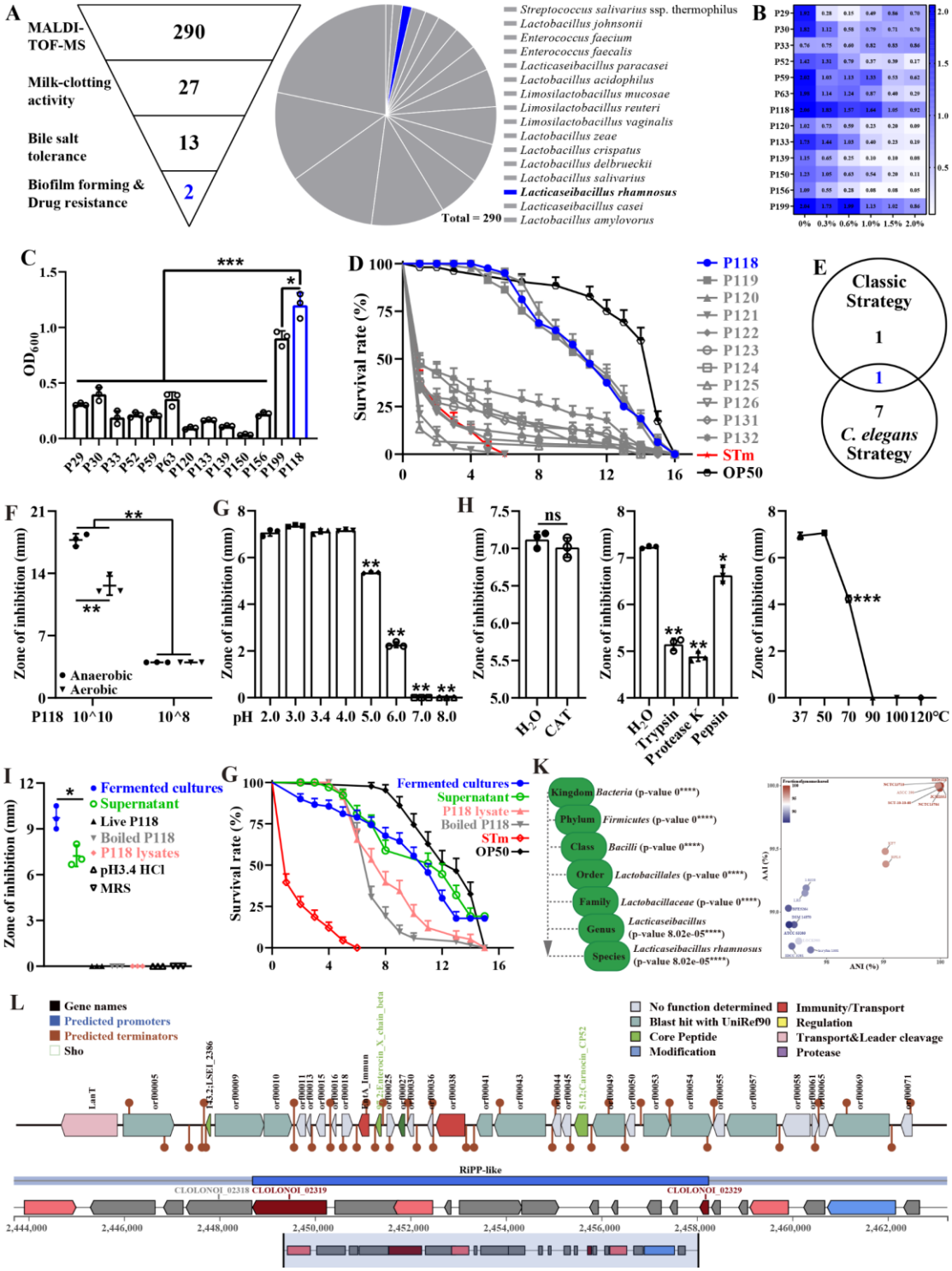

1004

1005 **Figure 1.** Isolation and antibacterial characterization of *L. rhamnosus* P118. (**A**)

1006 Screening flowchart of P118 *in vitro* and candidate probiotic isolates identified by

1007 MALDI-TOF MS. (**B**) Bile salt tolerance ability of the isolates. (**C**) Biofilm forming

1008 ability of isolates. (**D**) Screening using *C. elegans* infection model. (**E**) Interacted
1009 screening strategy. (**F**) Antibacterial ability of P118 under aerobic or anaerobic culture
1010 conditions. (**G**) Broad-spectrum pH tolerance of P118 supernatants (pH = 3.4) that
1011 adjusted to pH < 3.4 by 1M HCl or pH > 3.4 by 1M NaOH. (**H**) Antibacterial effects of
1012 P118 supernatant under 20 mg/mL catalase (CAT), 100μg/mL proteinases (trypsin,
1013 proteinase K, pepsin), and different temperatures (37, 50, 70, 90, 100, 120℃) boiled
1014 for 30 min treatments. (**I**) Antibacterial effects of components of P118 (boiled at 120 ℃
1015 for 30 min or was lysed by ultrasonication at 240 W for 2 h). (**G**) Active ingredients of
1016 P118 protect *C. elegans* against *S.* Typhimurium infection. (**K**) Taxonomic
1017 classification of P118 draft genome queried against the NCBI non-redundant
1018 prokaryotic genomes database with p-values representing confidence of phylogenetic
1019 assignment, and the nearest subspecies phylogenetic neighbor of P118 draft genome
1020 was determined by percentage shared genomic content graphed as ANI versus AAI. (**L**)
1021 Prediction of secondary metabolites and bacteriocin protein-encoding gene clusters of
1022 P118 using antiSMASH and BAGEL4 databases. (**F-G**) *S.* Typhimurium SL1344 was
1023 selected as an indicator pathogen. Significant differences * $P < 0.05$, ** $P < 0.01$, ***
1024 $P < 0.001$.

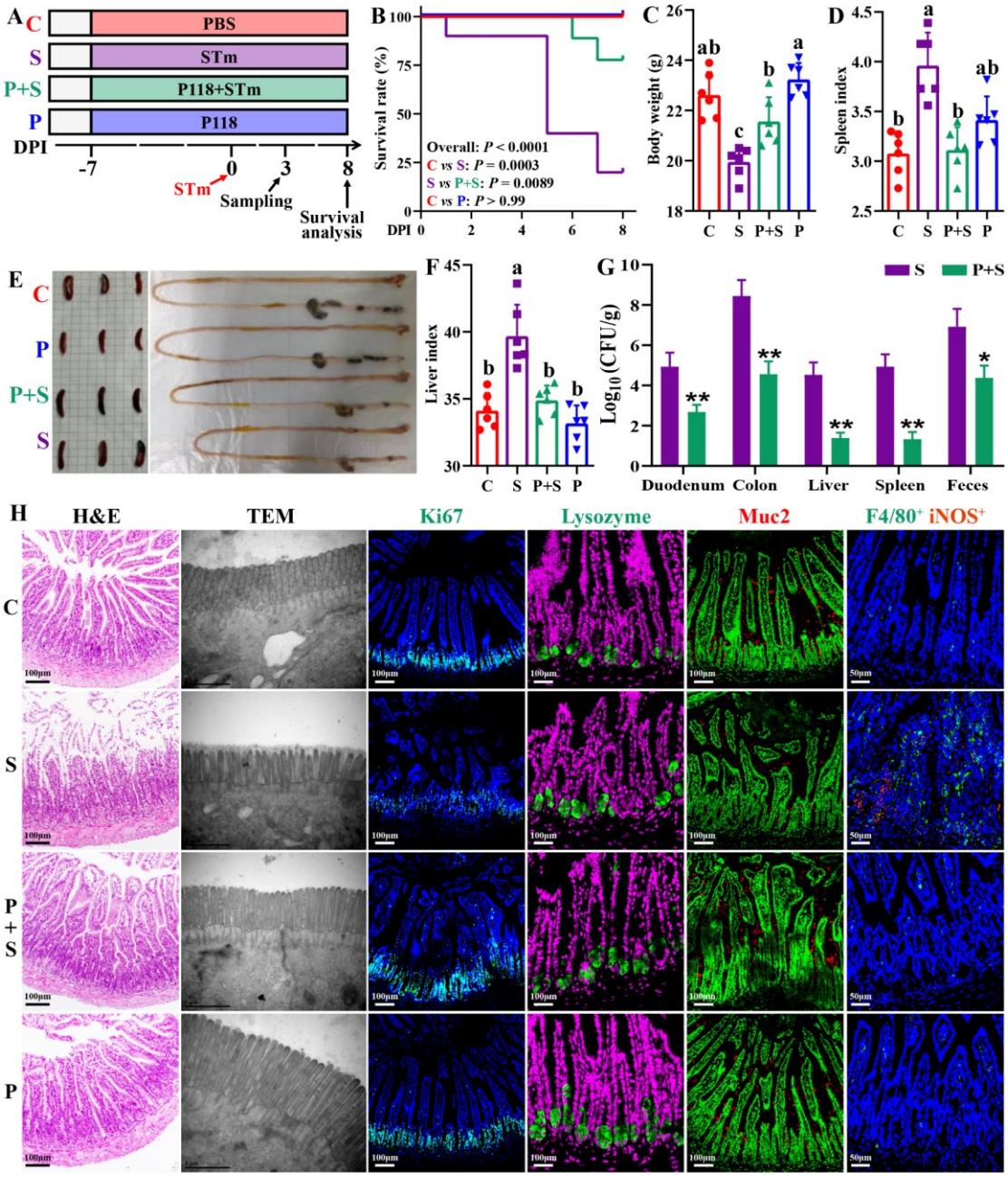

Figure 2. *L. rhamnosus* P118 enhances mice tolerance to *S*. Typhimurium infection. (**A**) Experimental design. (**B**) Survival curve of mice infected with *S*. Typhimurium. (**C**) Body weight. (**D**) Spleen index. (**E**) Representative images of spleen and intestine. (**F**) Liver index. (**G**) *S.* Typhimurium burden in tissues and shedding in feces. (**H**) Representative images of H&E staining, TEM, and immunostaining (DAPI, Ki67, lysozyme, Muc2, F4/80, iNOS) in the ileum. Different lowercase letters indicate a significant difference ($P < 0.05$). Significant differences * $P < 0.05$, ** $P < 0.01$. C:

PBS group; P: P118 administered group; S: *S*. Typhimurium-infected group; P+S: P118 protective group.

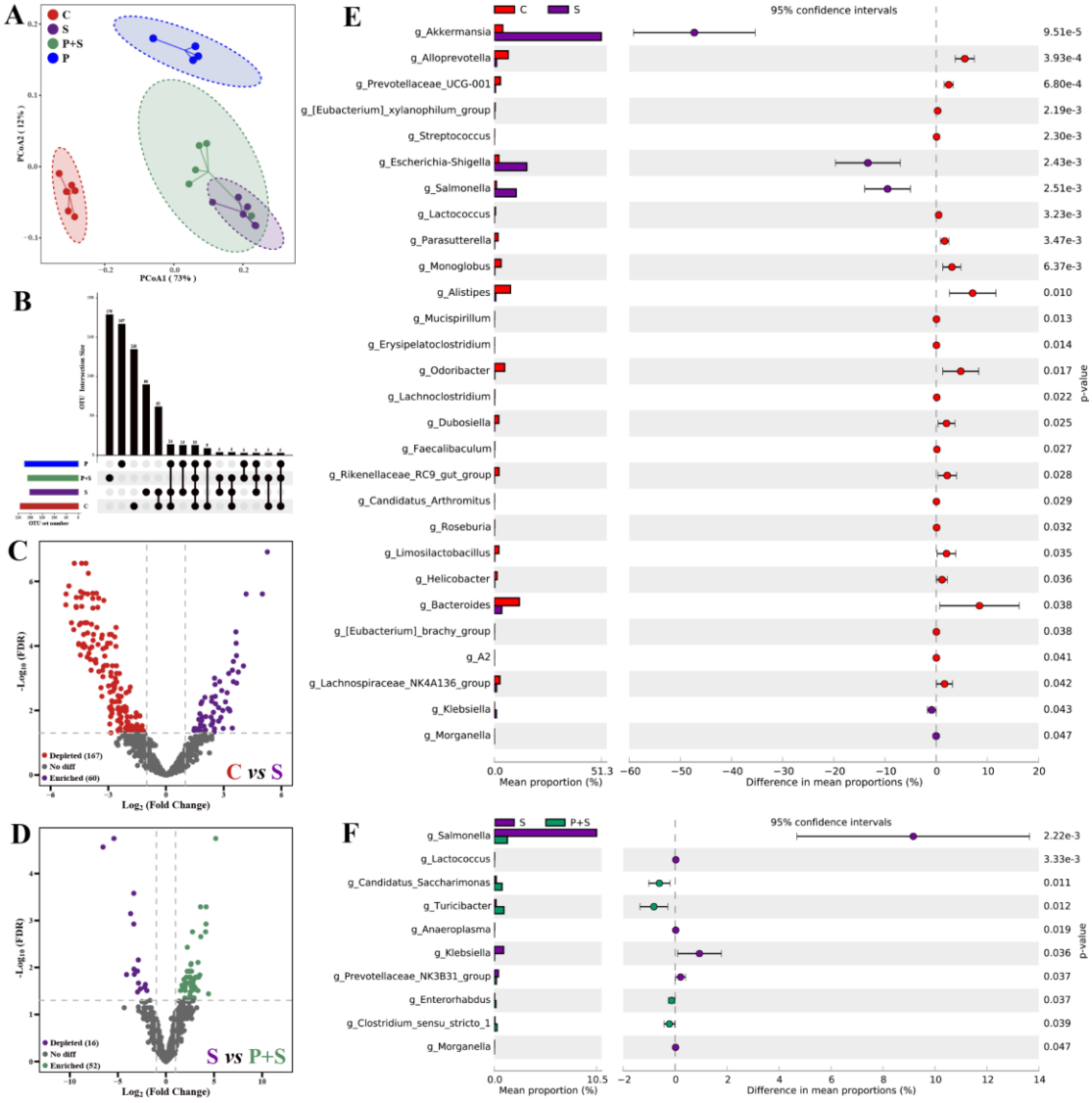

Figure 3. *L. rhamnosus* P118 improves *S*. Typhimurium infection-induced dysbacteriosis. (**A**) Principal coordinates analysis (PCoA) based on Bray-Curtis distance. (**B**) UpSetR plot based on bacterial absolute OTU abundances. (**C & D**) The fold changes of bacterial absolute OTU abundances between two groups. (**E & F**) Comparison of intestinal microbes by STAMP. The prefix "g_" represent the annotated level of the genus. C: PBS group; P: P118 administered group; S: *S*. Typhimurium-infected group; P+S: P118 protective group.

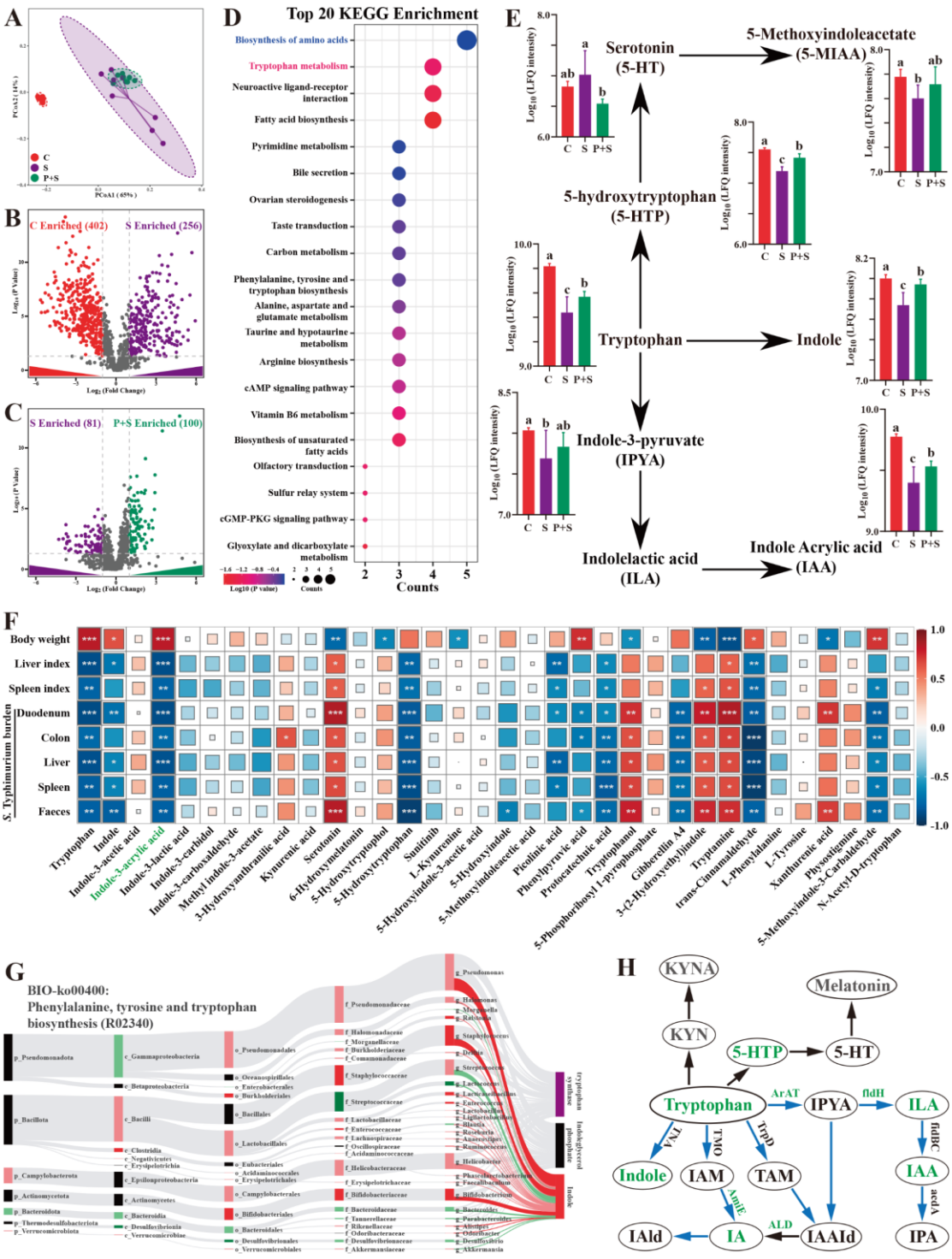

Figure 4. Microbe derived tryptophan metabolites are involved in mice tolerance to *S.* Typhimurium. (**A**) Principal coordinates analysis (PCoA) based on Bray-Curtis distance of fecal metabolites. (**B & C**) UpSetR plot based on fecal metabolites. (**D**) Metabolomics pathway enrichment in "P+S *vs* S". (**E**) Comparison of fecal microbial

tryptophan metabolism enriched pathway among groups. (**F**) Pearson correlation analysis among *S.* Typhimurium burden, organ indices, body weight and fecal metabolites in mice. (**G**) Bio-Sankey network analysis between intestinal microbes and fecal metabolites. (**H**) Pathway schematic of abbreviated mammalian and microbial tryptophan metabolism. Different lowercase letters indicate a significant difference ($P < 0.05$). Significant differences $^{*}P < 0.05$; $^{**}P < 0.01$; $^{***}P < 0.001$. C: PBS group; P: P118 administered group; S: *S.* Typhimurium-infected group; P+S: P118 protective group.

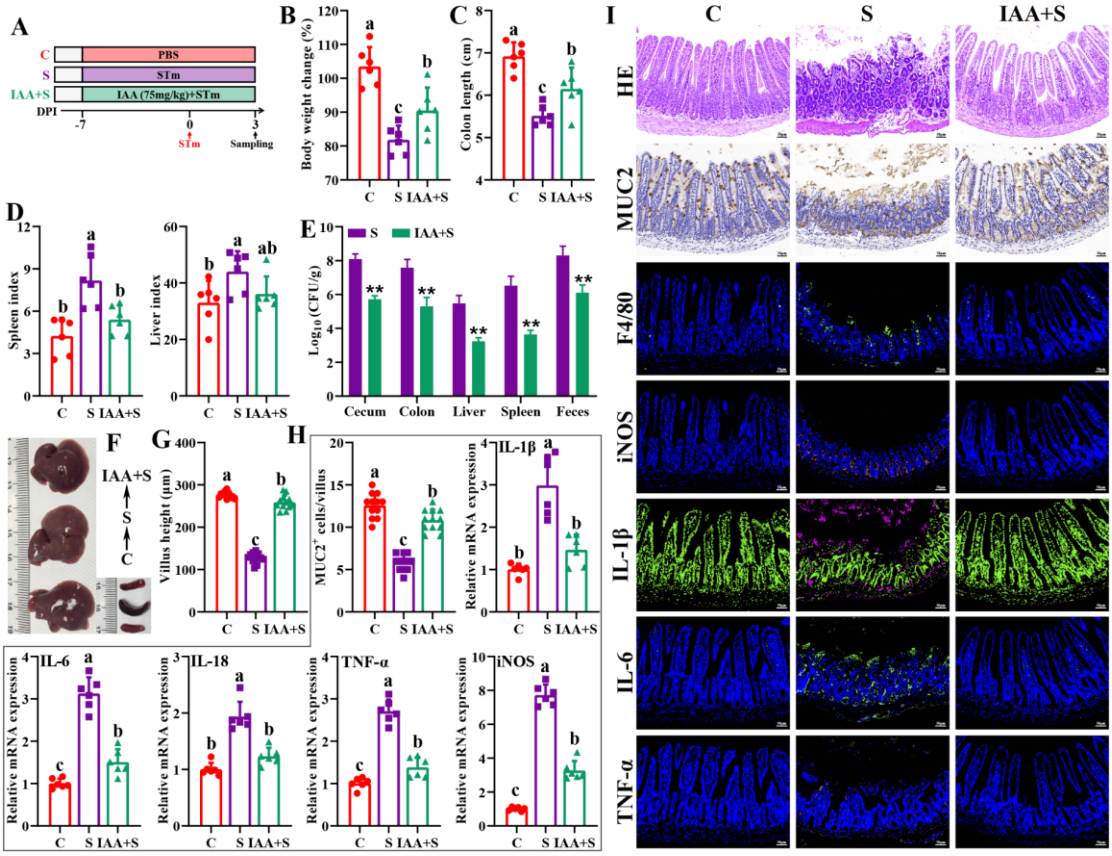

Figure 5. Indole-3-acrylic acid enhances mice tolerance to *S.* Typhimurium infection. (**A**) Experimental design. (**B**) Body weight change. (**C**) Colon length. (**D**) Spleen and liver indexes. (**E**) *S.* Typhimurium burden in tissues and shedding in feces. (**F**) Representative images of spleen and liver. (**G**) Villus height of ileum. (**H**) Muc2-

positive cells and mRNA expression levels in ileum. (**I**) Representative images of H&E staining and immunostaining in the ileum. Different lowercase letters indicate a significant difference ($P < 0.05$). C: PBS group; S: *S.* Typhimurium-infected group; IAA+S: indole-3-acrylic acid protective group.

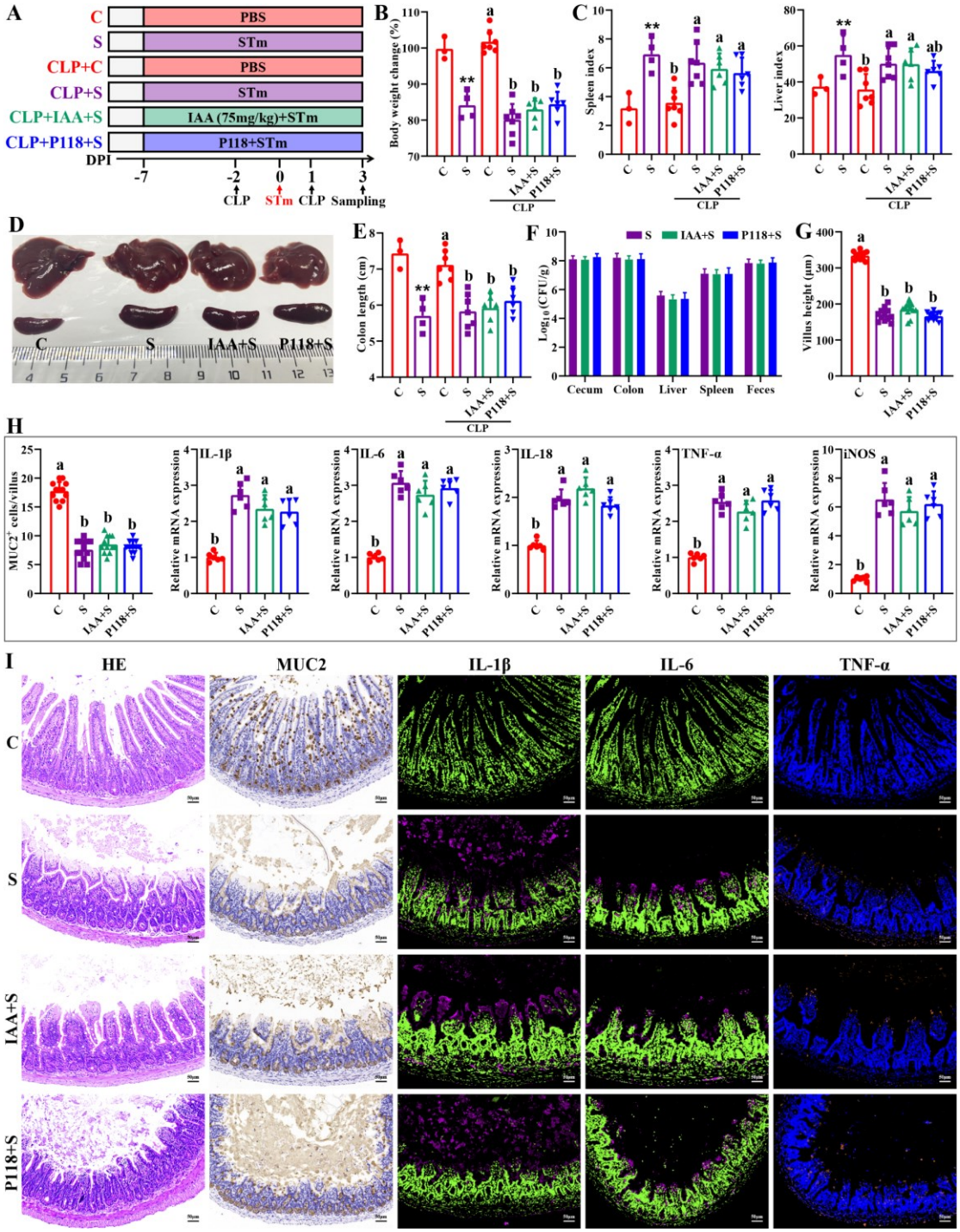

Figure 6. Macrophage depletion abrogates the protective effect of *L. rhamnosus* P118

and indole-3-acrylic acid against *S*. Typhimurium infection. (**A**) Experimental design. (**B**) Body weight change. (**C**) Spleen and liver indexes. (**D**) Representative images of spleen and liver. (**E**) Colon length. (**F**) *S.* Typhimurium burden in tissues and shedding in feces. (**G**) Villus height of ileum. (**H**) Muc2-positive cells and mRNA expression levels in ileum. (**I**) Representative images of H&E staining and immunostaining in the ileum. Different lowercase letters indicate a significant difference ($P < 0.05$). (**B-E**) Significant differences ** $P < 0.01$ indicates "S *vs* C".CLP: macrophage depletion reagent clodronate liposomes. C: PBS group; S: S. Typhimurium-infected group; IAA+S: indole-3-acrylic acid protective group; P+S: P118 protective group.

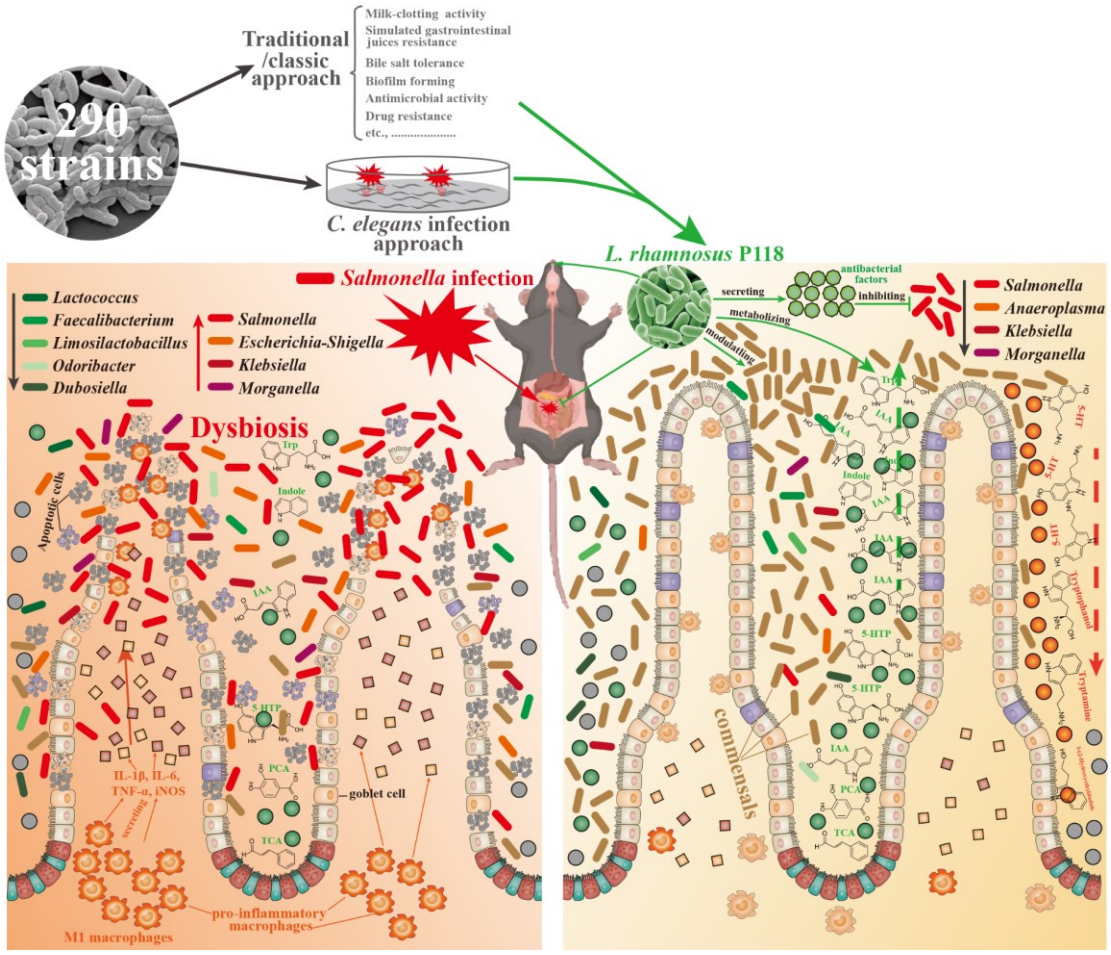

Figure 7. *Lacticaseibacillus rhamnosus* P118 strain with great probiotic properties was screened from 290 purified isolates through two distinctive screen approaches, and

1079 P118 strain was underscored for protective effects on a murine infection model. Further,
1080 multi-omics analysis pinpointed the microbe-derived tryptophan/indole could be the
1081 importance of P118 probiotic properties. Nevertheless, the newly found P118 enhances
1082 host tolerance to *Salmonella* infections via various pathways, including direct
1083 antibacterial actions, inhibiting *Salmonella* colonization and invasion, attenuating pro-
1084 inflammatory responses of intestinal macrophages, and modulating gut microbiota
1085 mediated by microbe-derived indole metabolites.

1086

1087

1088 **Table 1** A list of probiotic isolates recovered from examined samples

Source	Name	Number of isolates
Yogurt	*Streptococcus salivarius ssp. thermophilus*	63
	Lacticaseibacillus paracasei	18
	Lactobacillus acidophilus	17
	Lactobacillus zeae	10
	Lacticaseibacillus rhamnosus	4
	Lacticaseibacillus casei	4
	Lactobacillus delbrueckii	6
piglet intestine	*Limosilactobacillus mucosae*	16
	Lactobacillus johnsonii	38
	Limosilactobacillus reuteri	16
	Limosilactobacillus vaginalis	11
	Lactobacillus crispatus	9
	Lactobacillus salivarius	6
	Lactobacillus amylovorus	3
	Enterococcus faecium	38
	Enterococcus faecalis	31
Total		290

1089 **Supplementary information**

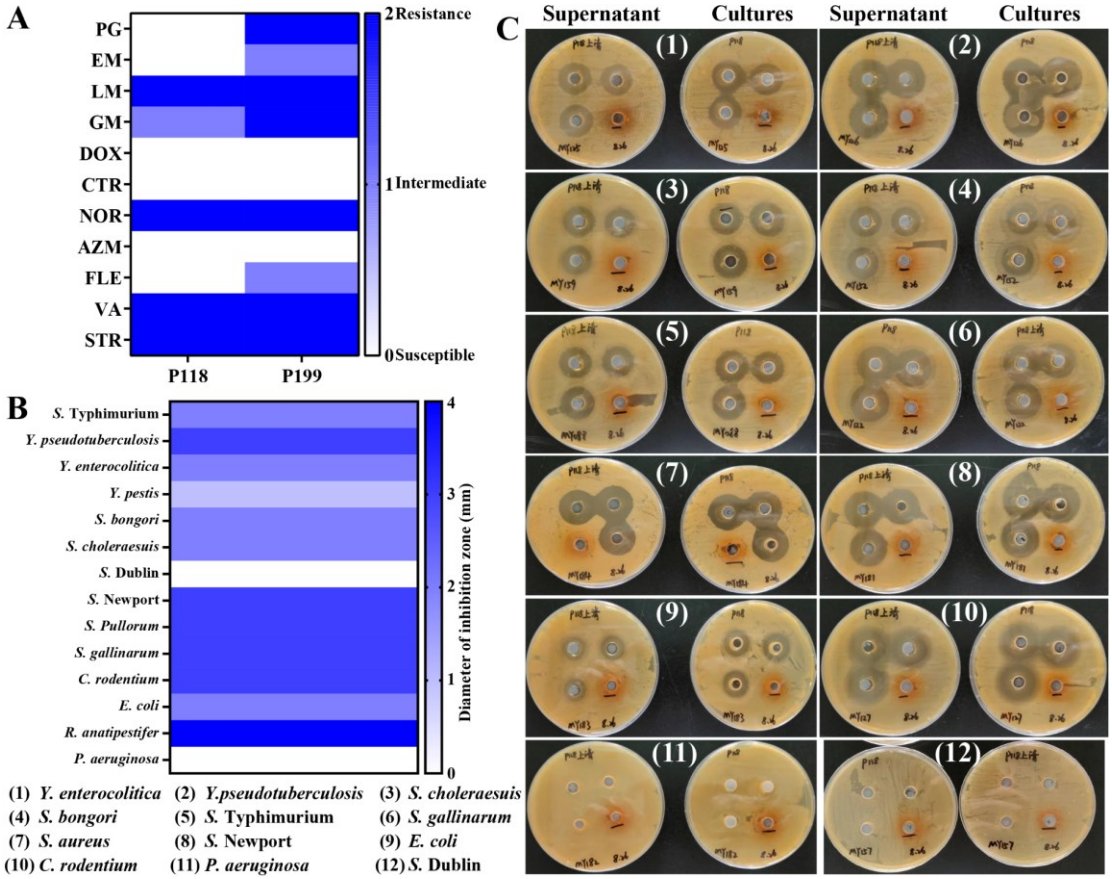

Figure S1 (**A**) Drug resistance candidate probiotic isolates (P118 and P199). (**B, C**) Broad-spectrum antibacterial activities of P118 fermented supernatants and cultures.

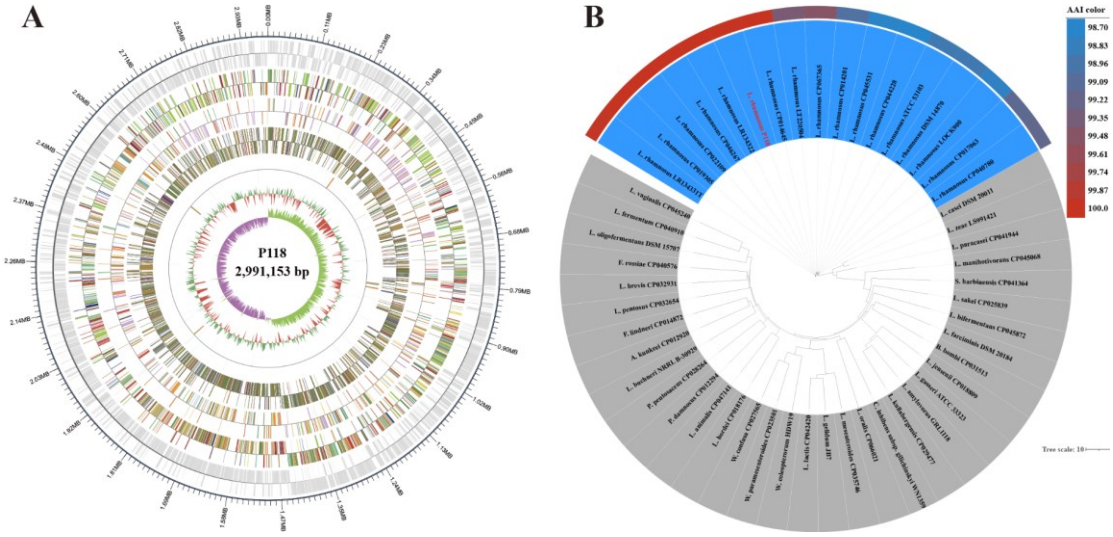

Figure S2. (**A**) Circular genome map of *L. rhamnosus* P118. (**B**) phylogenetic trees of *L. rhamnosus* P118 and nearest phylogenetic neighbors constructed by average amino acid identify (AAI). Color gradients indicate the percentage of conserved average

nucleotide identity (ANI) between each isolate and respective nearest subspecies phylogenetic neighbors.

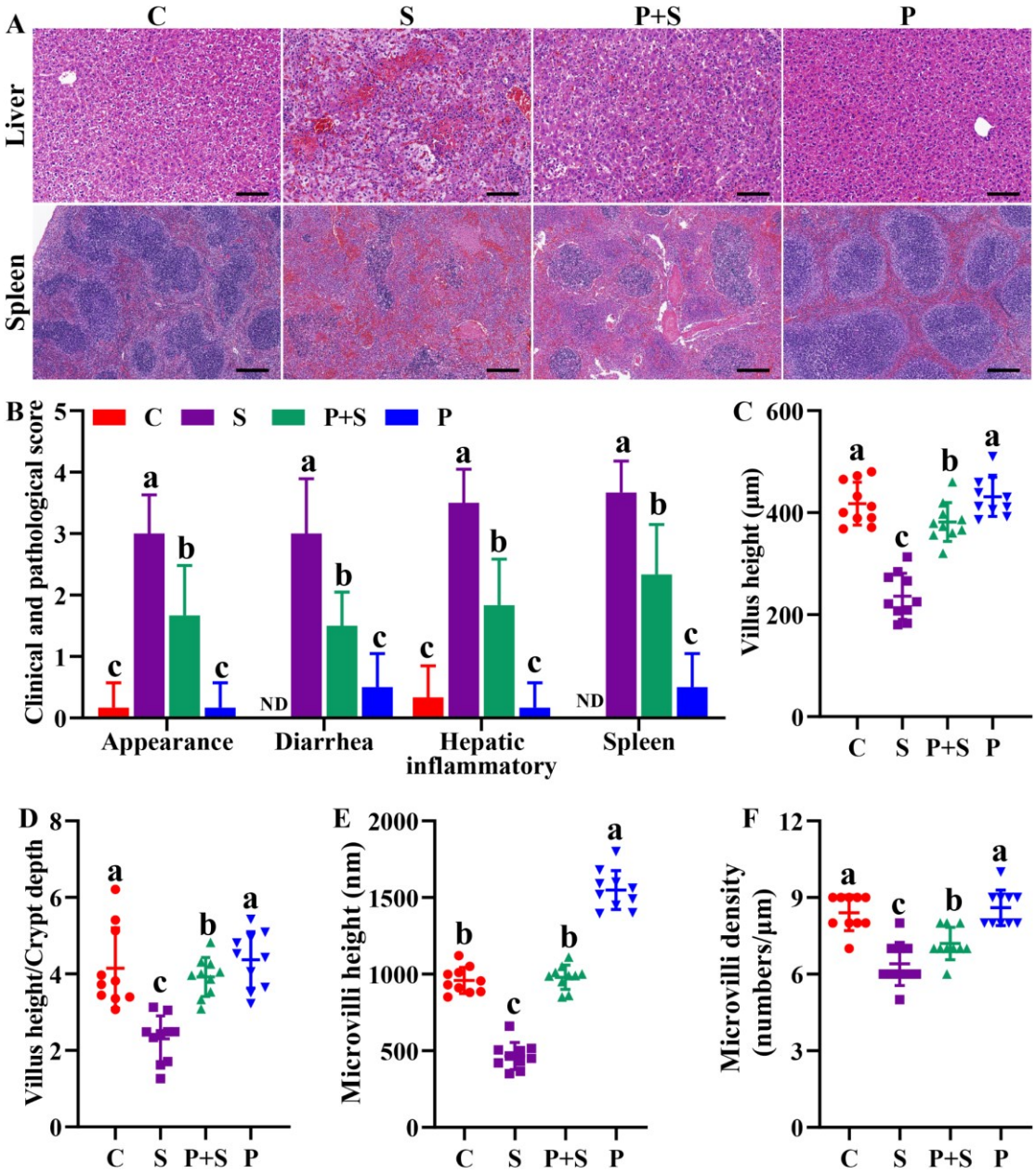

Figure S3. Clinical and Histopathological observation. (**A**) Representative images of H&E staining tissues (liver, spleen). Scale bar with 100 μm. (**B**) Clinical symptom score. Histopathological quantification of H&E staining (**C & D**) and TEM (**E & F**) images observed in the ileum. Different lowercase letters indicate a significant difference ($P < 0.05$). C: PBS group; P: P118 administered group; S: *S*. Typhimurium-infected group;

1105 P+S: P118 protective group.

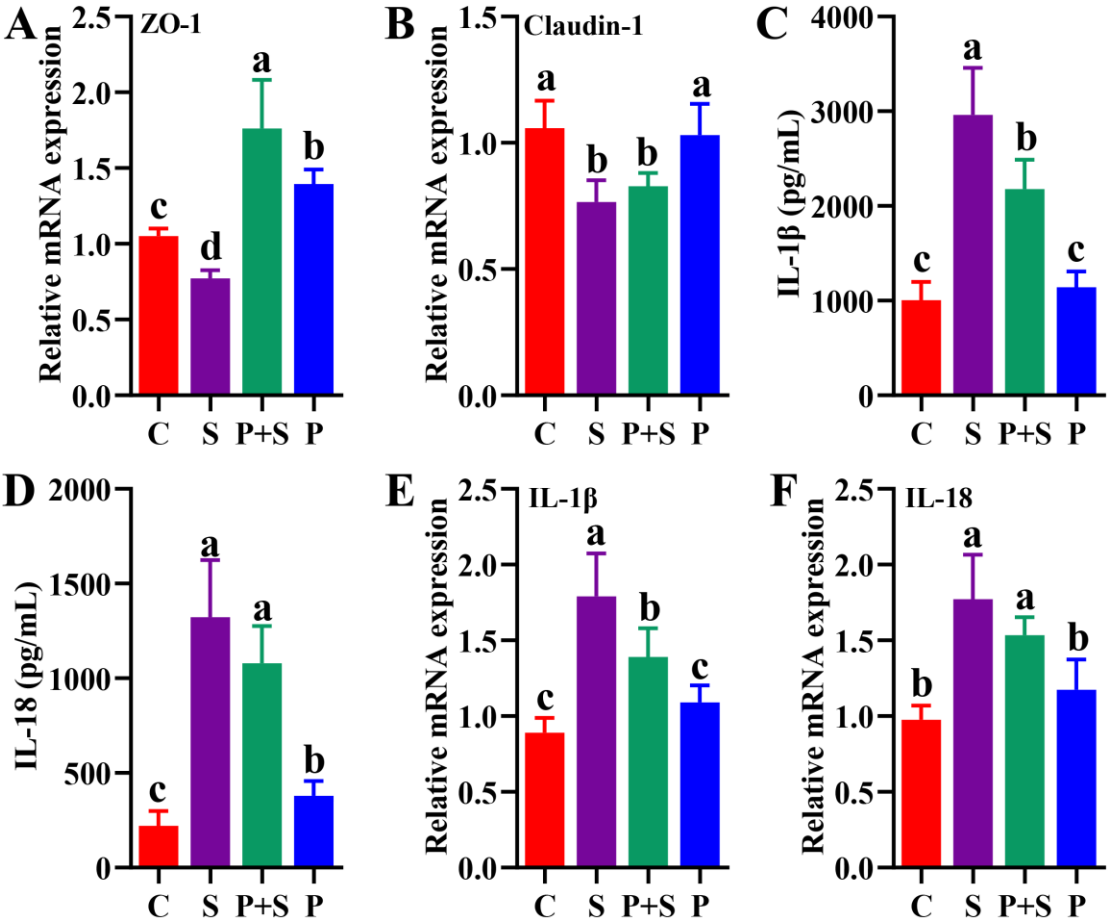

1106

1107 **Figure S4.** Gene and protein expression level of tight junction protein (ZO-1, Claudin-

1108 1) and inflammatory cytokines (IL-1β, IL-18) in ileum and serum of mice. Different

1109 lowercase letters indicate a significant difference ($P < 0.05$). C: PBS group; P: P118

1110 administered group; S: *S*. Typhimurium-infected group; P+S: P118 protective group.

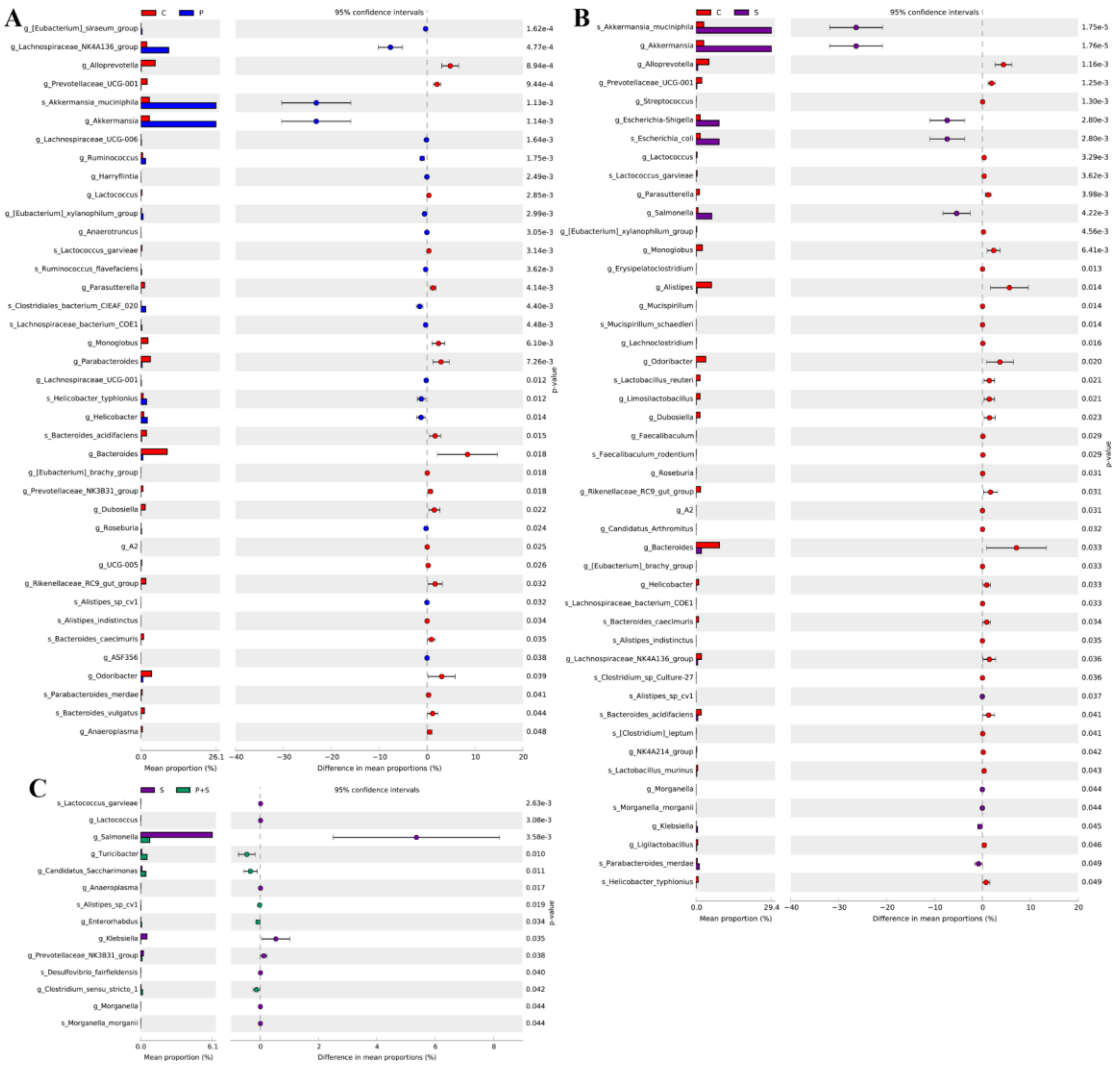

Figure S5. Comparison of intestinal microbes by the analysis of statistical analysis of taxonomic and functional profiles (**STAMP**) software with a two-sided Welch's t-test. (**A**) C *vs* P, (**B**) C *vs* S, (**C**) S *vs* P+S. The prefixes "g_" and "s_" represent the annotated levels of genus and species. C: PBS group; P: P118 administered group; S: *S.* Typhimurium-infected group; P+S: P118 protective group.

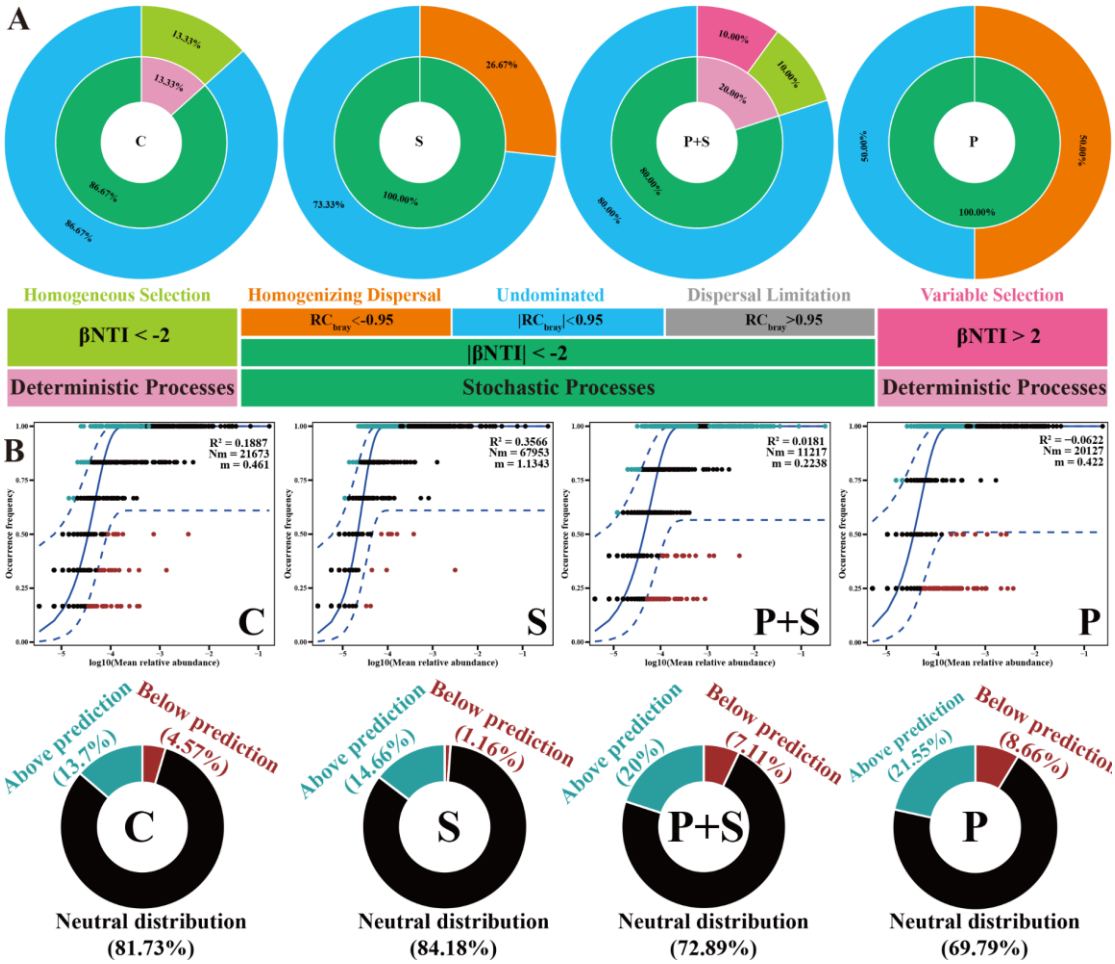

Figure S6. *L. rhamnosus* P118 alters gut microbial community assembly. (**A**) Ecological processes of gut microbes. The inner circle indicates the percentage of deterministic and stochastic assembly processes. The outer circle indicates the contribution of detailed ecological processes. **(B)** The fit of neutral community model (NCM) of community assembly for gut microbes. The best fit to NCM and 95% CIs around the best fit to NCM were indicated by solid and dashed blue lines, respectively. Light blue and dark red dots indicate OTUs that occur more (above prediction) or less (below prediction) frequently than predicted by NCM, respectively, while black dots indicate the OTUs that occur within neutral prediction (neutral distribution). Donut charts shows the distinct fitting proportions of OTUs predicted by NCM. C: PBS group; P: P118 administered group; S: *S.* Typhimurium-infected group; P+S: P118 protective

group.

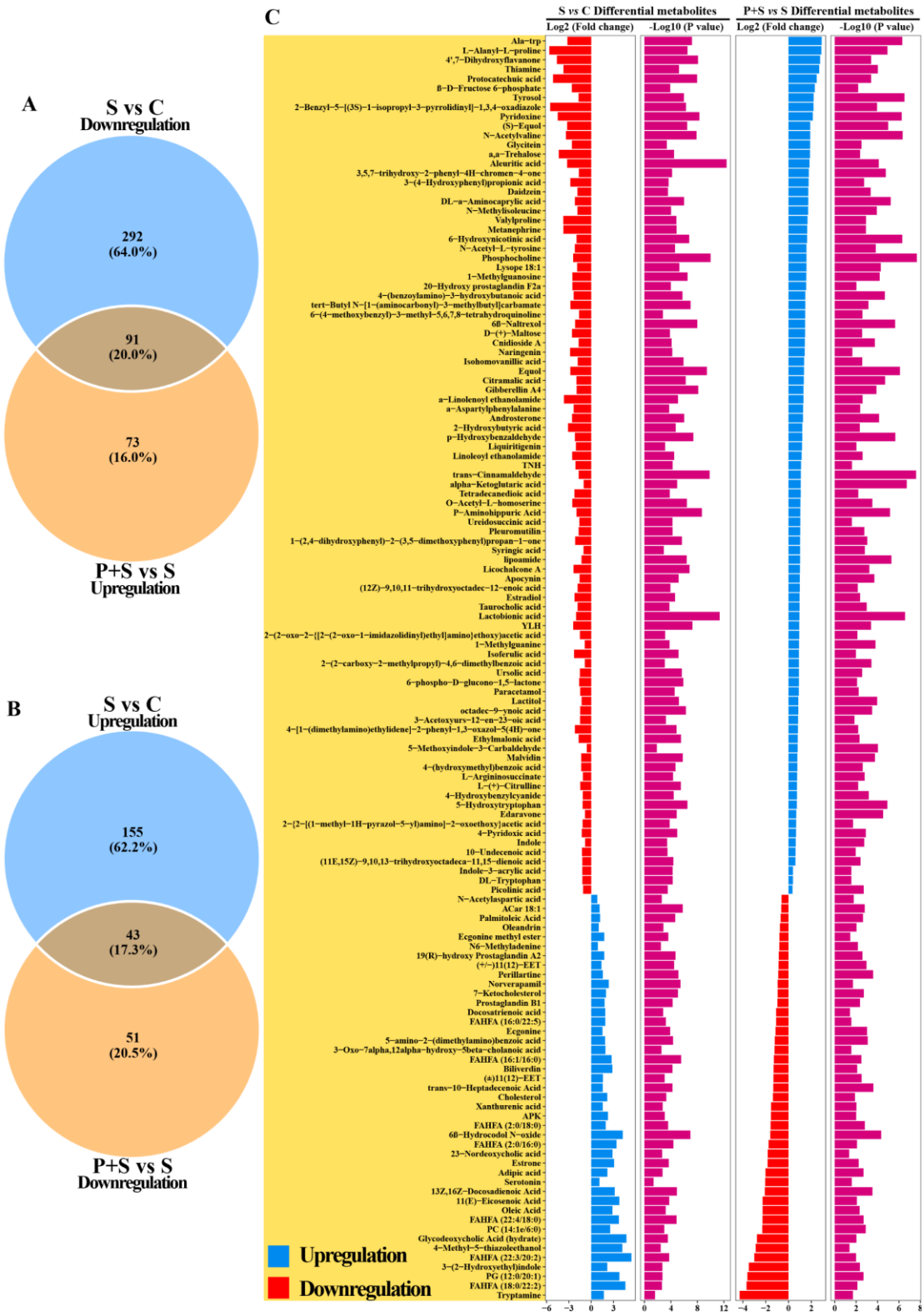

Figure S7. Analysis of differential fecal metabolites. Venn diagram based on

differential fecal metabolites (**A**) down-regulated in "S *vs* C" and up-regulated in "P+S *vs* S", (**B**) up-regulated in "S *vs* C" and down-regulated in "P+S *vs* S". (**C**) Significant differential fecal metabolites in "S *vs* C" and "P+S *vs* S". C: PBS group; P: P118 administered group; S: *S*. Typhimurium-infected group; P+S: P118 protective group.

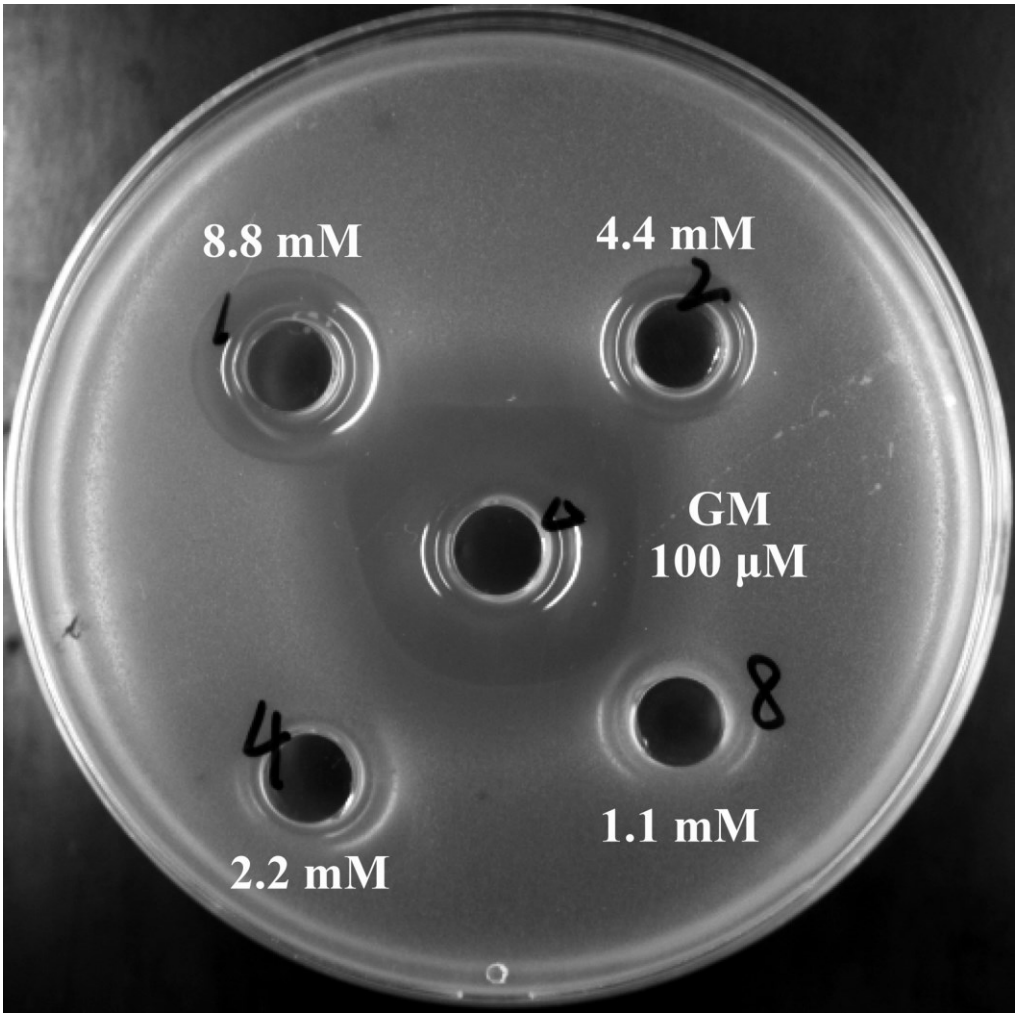

Figure S8. Antibacterial activities of indole-3-acrylic acid. GM: 100 μg/mL gentamicin.

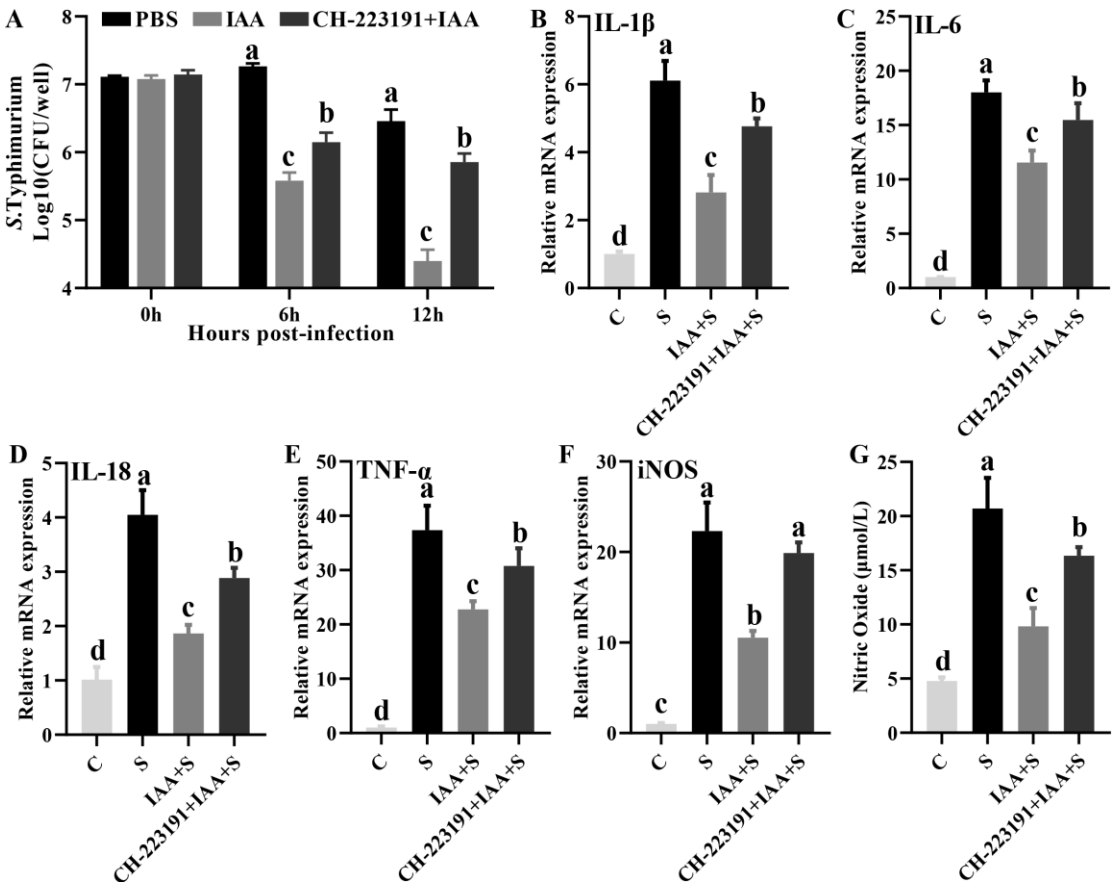

Figure S9. Indole-3-acrylic acid enhances bactericidal capacity and exerts anti-inflammatory activity in RAW 264.7 cells. Different lowercase letters (a, b, c, d) indicate a significant difference ($P < 0.05$). C: PBS group; IAA: indole-3-acrylic acid group; S: *S*. Typhimurium-infected group; CH-223191: AHR inhibitor-treated group.

Table S1 Milk-clotting activity of lactic acid bacteria

Table S2 Significance between life span data was calculated using a Mantel-Cox log-rank test

Table S3 Significance between life span data was calculated using a Mantel-Cox log-rank test

Table S4 Species-level identity of *L. rhamnosus* P118. The draft genome of P118 was queried using the NCBI non-redundant prokaryotic database available through MIGA

1152 (http://www.microbial-genomes.org). P-values reflect confidence in the assignment as
1153 each taxonomic rank.

1154 **Table S5** *L. rhamnosus* P118 draft genome nearest subspecies phylogenetic neighbors.
1155 Average nucleotide identity (ANI) and average amino acid identity (AAI) using both
1156 percent identity and a fraction of genome shared as determined through MIGA
1157 (http://www.microbial-genomes.org) query of the NCBI non-redundant prokaryotic
1158 genomes database were considered for ranking likelihood of nearest subspecies
1159 phylogenetic neighbors for duplicate isolates of each *Lacticaseibacillus* species.

1160 **Table S6** Primers used for the quantitative PCR

1161 **Table S7** The criteria of clinical symptom scores

1162 **Table S8** ANOSIM, PERMANOVA and MRPP analysis of microbial diversity among
1163 treatments

1164 **Table S9** ANOSIM, PERMANOVA and MRPP analysis of fecal metabolites among
1165 groups

1166 **Table S10** Significant differential fecal metabolites in "S *vs* C" and "P+S *vs* S"

1167 **Table S11** Prediction of aminotransferase class and tryptophan binding affinity in *L.*
1168 *rhamnosus* P118

1169 **Table S12** Tryptophan metabolism and indole derivatives in *L. rhamnosus* P118
1170 cultures